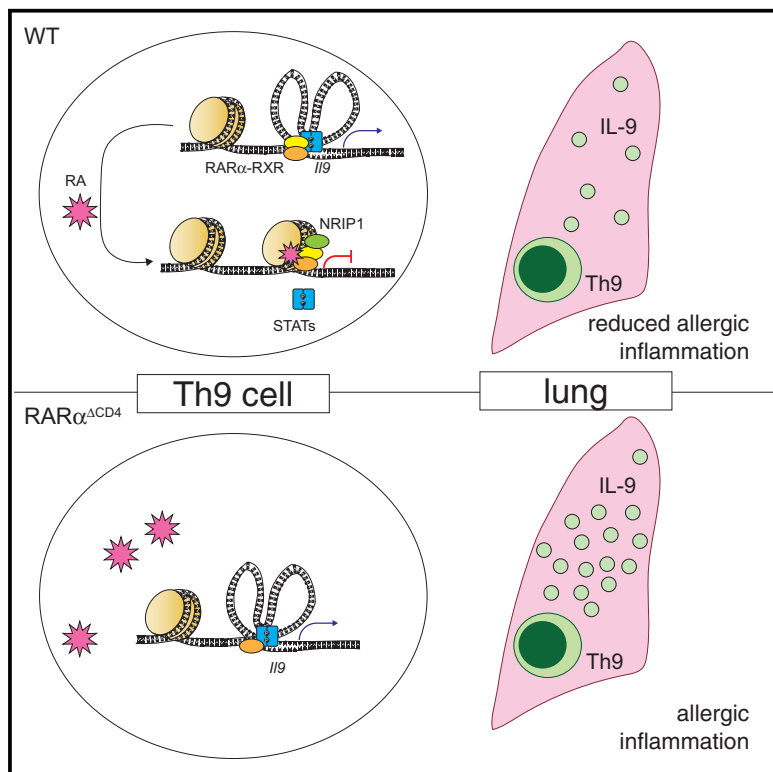


Retinoic Acid Receptor Alpha Represses a Th9 Transcriptional and Epigenomic Program to Reduce Allergic Pathology

Graphical Abstract



Authors

Daniella M. Schwartz, Taylor K. Farley,
Nathan Richoz, ..., Arian Laurence,
Françoise Meylan, John J. O'Shea

Correspondence

daniella.schwartz@nih.gov

In Brief

Schwartz et al. examine the impact of retinoic acid (RA) on the genome-wide transcriptional response during differentiation of CD4 $^{+}$ T cells to different Th subsets, revealing a role for RA in repressing the Th9 differentiation program. Their findings argue for the importance of this dietary metabolite in immune homeostasis and in Th9-associated inflammatory disease.

Highlights

- Global effects of retinoic acid (RA) were evaluated by RNA sequencing in major Th subsets
- RA impacts the transcriptome of Th9 cells more so than that of other effector subsets
- RA-RAR α represses the *Il9* locus and Th9 program independently of Foxp3
- RA-RAR α activity controls pathology in Th9-associated allergic lung disease



Retinoic Acid Receptor Alpha Represses a Th9 Transcriptional and Epigenomic Program to Reduce Allergic Pathology

Daniella M. Schwartz,^{1,5,9,*} Taylor K. Farley,^{2,6} Nathan Richoz,² Chen Yao,¹ Han-Yu Shih,¹ Franziska Petermann,¹ Yuan Zhang,⁵ Hong-Wei Sun,³ Erika Hayes,² Yohei Mikami,^{1,7} Kan Jiang,¹ Fred P. Davis,¹ Yuka Kanno,¹ Joshua D. Milner,⁵ Richard Siegel,² Arian Laurence,⁴ Françoise Meylan,^{2,8} and John J. O'Shea^{1,8}

¹Molecular Immunology and Inflammation Branch, NIAMS, NIH, Rockville, MD 20892, USA

²Immunoregulation Section, Autoimmunity Branch, NIAMS, NIH, Rockville, MD 20892, USA

³Office of Science and Technology, NIAMS, NIH, Rockville, MD 20892, USA

⁴Translational Gastroenterology Unit, Experimental Medicine Division, John Radcliffe Hospital, University of Oxford, UK

⁵Genetics and Pathogenesis of Allergy Section, Laboratory of Allergic Diseases, NIAID, NIH, Rockville, MD 20892, USA

⁶Metaorganism Immunity Section, Laboratory of Immune System Biology, NIAID, NIH, Rockville, MD 20892, USA

⁷Present address: Division of Gastroenterology and Hepatology, Department of Internal Medicine, Keio University School of Medicine, Tokyo, Japan

^{*}Senior author

⁹Lead Contact

*Correspondence: daniella.schwartz@nih.gov

<https://doi.org/10.1016/j.immuni.2018.12.014>

SUMMARY

CD4⁺ T helper (Th) differentiation is regulated by diverse inputs, including the vitamin A metabolite retinoic acid (RA). RA acts through its receptor RAR α to repress transcription of inflammatory cytokines, but is also essential for Th-mediated immunity, indicating complex effects of RA on Th specification and the outcome of the immune response. We examined the impact of RA on the genome-wide transcriptional response during Th differentiation to multiple subsets. RA effects were subset-selective and were most significant in Th9 cells. RA globally antagonized Th9-promoting transcription factors and inhibited Th9 differentiation. RA directly targeted the extended *Il9* locus and broadly modified the Th9 epigenome through RAR α . RA-RAR α activity limited murine Th9-associated pulmonary inflammation, and human allergic inflammation was associated with reduced expression of RA target genes. Thus, repression of the Th9 program is a major function of RA-RAR α signaling in Th differentiation, arguing for a role for RA in interleukin 9 (IL-9) related diseases.

INTRODUCTION

CD4⁺ T cells are critical orchestrators of immune responses, and different T helper (Th) subsets direct responses to specific pathogens (Abbas et al., 1996; Dong and Flavell, 2000; O'Shea and Paul, 2010). CD4⁺ fate decisions are influenced by environmental immunomodulators—including cytokines, microbiota, and metabolites—that signal through diverse receptors (Josefowicz and Rudensky, 2009; Miossec et al., 2009). Retinoic acid (RA),

a metabolite synthesized from dietary vitamin A by cell-specific dehydrogenases, has essential roles in human health that include broad effects on hematopoietic lineage decisions and immune cell function (Hall et al., 2011b; Phan et al., 2017). In mucosal and lymphoid tissues, RA synthesized by dendritic cells acts on CD4⁺ T cells, signaling through nuclear receptors (RARs) to modulate Th differentiation and function (Benson et al., 2007; Mucida et al., 2007; Raverdeau and Mills, 2014). Inflammatory stimuli promote RA synthesis and increase RAR activity in Th cells (Iwata et al., 2004; Manicassamy et al., 2009; Pino-Lagos et al., 2011).

RA's role in Th-mediated immunity is complex, as illustrated by its numerous, seemingly contradictory effects (Larange and Cheron, 2016). RA is important for CD4⁺ T-effector (Teff) cell responses in some contexts, including defense from infection and response to immunization; but RA ameliorates CD4⁺-dependent autoimmune disease and suppresses Teff cytokines in other situations (Elias et al., 2008; Hall et al., 2011a; Kwok et al., 2012; Xiao et al., 2008). Several potential explanations are proposed for these inconsistencies, including concentration-dependent RA effects; context-dependent RA effects that vary in different Th subsets in different tissues; and indirect RA-mediated suppression of Teff differentiation via induction of the transcriptional regulator Forkhead Box P3 (Foxp3), a key mediator of peripheral tolerance (Hall et al., 2011b; Maynard et al., 2009; Mucida et al., 2007; Takahashi et al., 2012; Xiao et al., 2008). In recent years, various models of RAR deficiency have been used to investigate the molecular mechanisms underlying RA's effects on Th cells (Brown et al., 2015; Hall et al., 2011a; Reis et al., 2013), leading to important insights regarding the role of RA-RAR signaling in Th differentiation and function. Yet RA-RAR signaling has primarily been studied in the context of Th1 and Th17 responses, and its role in other Teff lineages is less characterized (Brown et al., 2015; Elias et al., 2008; Hall et al., 2011a; Kwok et al., 2012). This is particularly true for Th9 cells, which have recently emerged as important modulators of atopy, autoimmunity, and cancer (Kaplan et al., 2015). The factors governing Th9 specification are



not as well understood as those influencing the differentiation of other Th subsets (Kaplan, 2017). Nonetheless, Th9 cells promote allergic inflammation and reduce barrier immunity at mucosal surfaces, which are RA-rich microenvironments (Lorange and Cheroutre, 2016), suggesting that RA-RAR signaling might have a prominent role in the differentiation and function of this subset.

In this study, we broadly surveyed the transcriptomic effects of RA on the major Th subsets. *In vitro*, RA primarily had subset-selective effects and quantitatively regulated Th9 transcriptomes more than those of other effector subsets. Foxp3 was largely irrelevant for RA gene regulation in Th9 cells; instead, RA globally antagonized Th9-lineage-promoting transcription factors (TFs), consequently limiting the Th9 transcriptomic program. The RA receptor RAR α directly targeted the extended *Ilo* locus, promoted chromatin remodeling, and impaired TF binding to regulatory regions. *In vivo*, treatment with RA ameliorated Th9-associated lung inflammation in mice, whereas genetic deletion of RAR α exacerbated disease. Accordingly, allergic inflammation in human subjects was associated with reduced expression of RA target genes. Our findings establish that RA-RAR α directly represses the Th9 transcriptional program, arguing for a potential role for this essential dietary factor in controlling interleukin 9 (IL-9)-related diseases such as asthma.

RESULTS

RA Has a Quantitatively Greater Effect on Th9 and iTreg Transcriptomes Relative to Other Th Subsets

To gain insight into the effects of RA on diverse Th subsets, we first assessed its effects on the transcriptomes of CD4 $^{+}$ T cells differentiated *in vitro* under neutral (Th0), effector (Th1, Th2, Th9, Th17), and regulatory (iTreg) conditions. RA regulated 1,025 differentially expressed genes (DEGs) in >1 Th subset. Overall, the impact of RA was greater (>350 DEGs) in Th17, Th9, and iTreg cells compared to Th0, Th1, and Th2 cells (<250 DEGs) (Figure 1A). Only 326 DEGs (32%) were similarly regulated in ≥ 3 subsets (common): 225 induced and 101 repressed. Common RA-induced DEGs were enriched for RAR signaling (*Crabp2*, *Stra6*) and chemotaxis (*Ccr9*, *Itga4*), serving as a positive control because these genes are known to be RA regulated (Coombes et al., 2007; Iwata et al., 2004). By contrast, common RA-repressed DEGs were highly enriched for JAK-STAT signaling. RA both induced (*Nfatc1*, *Fos*) and repressed (*Cd24a*, *Icos*) genes important for leukocyte activation, potentially offering an explanation for RA's role as both a positive and a negative regulator of Teff function (Bai et al., 2004; Dong et al., 2001) (Figures 1B and S1A; Table S1).

RA regulated a larger number of DEGs (699, 68%) in a subset-selective fashion, either coordinately inducing or repressing expression in ≤ 2 subsets. RA selectively induced several genes that promote Th2 immunity (*Adam8*, *Sema7a*), Th1 cell function (*Cxcl10*, *Rsd2*), and Th17 function (*Ilo23a*, *Ilo22*) (Mizutani et al., 2015; Naus et al., 2010). RA repressed 105 DEGs in Th1 and/or Th17 cells; this included positive (*Cysltr1*, *Rbpj*) and negative (*Ets1*, *Ecm1*) regulators of Th17 function, consistent with RA's variable effects on Th17 specification (Lee et al., 2015; Meyer Zu Horste et al., 2016; Moisan et al., 2007; Su et al., 2016). Subset-selective induction of genes that are important for host defense helps explain RA's role in promoting CD4 $^{+}$ -mediated immunity, despite suppression of many Teff cytokines.

The largest group of 428 DEGs (42%) was regulated primarily in Th9 and iTreg cells (Figures 1B, S1B, and S1C). RA increased the transcription of genes related to transforming growth factor beta (TGF- β) signaling and Th17 differentiation, but repressed inflammatory genes involved in nuclear factor κ B (NF- κ B) and tumor necrosis factor (TNF) signaling. Several genes (*Casp3*, *S1pr1*, *Cd83*) repressed by RA in Th9 and iTreg were RA induced in Th17 cells, whereas some RA-induced genes (*Cd101*, *Tigit*, *Ramp1*) in Th9 and iTreg were repressed in Th17 cells; this may underlie some complexities of RA signaling. Taken together, these results indicate that RA has a major subset-specific effect on Th9 and iTreg cells.

RA Represses the Motif Accessibility, Expression, and Targets of Key Th9 Transcription Factors

Global chromatin accessibility is thought to provide a more stable view of cell state than exclusively assessing steady-state mRNA expression (Shih et al., 2016). Because RA's major effect was on Th9 cells, we hypothesized that changes in chromatin accessibility would better define the role of RA in this subset. We measured global chromatin accessibility by ATAC-seq (assay for transposase-accessible chromatin using sequencing) with *in vitro* generated Th9 cells, including iTreg cells as a comparator because RA had similar effects in this subset. RA treatment caused the gain of 17,362 ATAC peaks and the loss of 6,756 peaks under Th9 conditions, and the gain of 15,283 peaks and the loss of 6,112 peaks under iTreg conditions, compared to control-treated cells (Figure 2A).

To identify transcription factors (TFs) that might mediate the actions of RA, we searched for differential motif abundance in peaks gained versus peaks lost upon RA treatment. 52 TF binding motifs were differentially enriched in Th9-promoting conditions, and 63 motifs were differentially enriched in iTreg-promoting conditions (Figure 2A). Of these, RA increased both the expression and the motif enrichment of 12 TFs in either iTreg-promoting conditions, Th9-promoting conditions, or both (USF2, FLI1, FOXP1, TCF12, JUN, RORC, NFATC1, VDR, BACH2, SMAD3, CTCF, RUNX1).

To confirm the relevance of these findings, we investigated RA effects on the targets of these TFs. We first identified 7 RA-induced TFs for which we could generate target-gene lists using public gene-expression data (TF deletion or overexpression). We then measured the average, or net, effect of RA on each target gene-set, using gene set enrichment analysis (GSEA) (Subramanian et al., 2005). RA had the same effect as RUNX1 in both Th9- and iTreg-promoting conditions, inducing RUNX1-induced genes and repressing RUNX1-repressed genes. Findings were similar for SMAD3 targets, but there was no consistent RA effect on the other target gene-sets (Figure 2B).

Conversely, RA reduced the expression and the motif enrichment of 10 TFs in either iTreg-promoting conditions, Th9-promoting conditions, or both (RXR α , FOSL2, IRF4, BATF, ATF3, NF κ B-p52, NF κ B-p65, STAT5a, STAT6, GATA3). Investigating the net effect of RA on target genes of these TFs revealed no consistent effect on BATF, FOSL2, or ATF3 targets (Figure 2B). However, RA had a net effect of repressing STAT5-induced genes and of inducing STAT5-repressed genes, in both Th9 and iTreg conditions. Results were similar for STAT6, GATA3, and NF- κ B targets in Th9 and iTreg conditions, and for IRF4 target

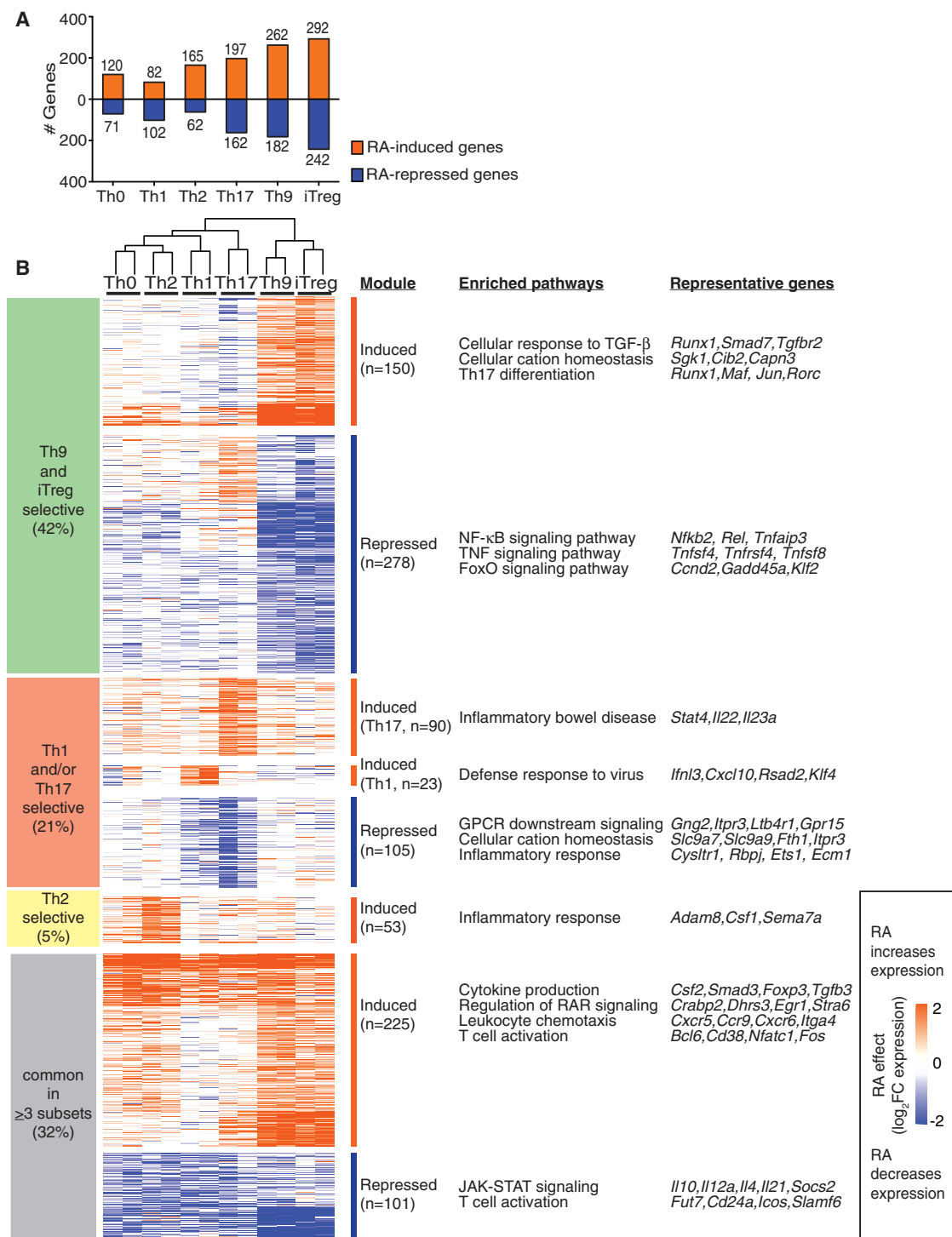
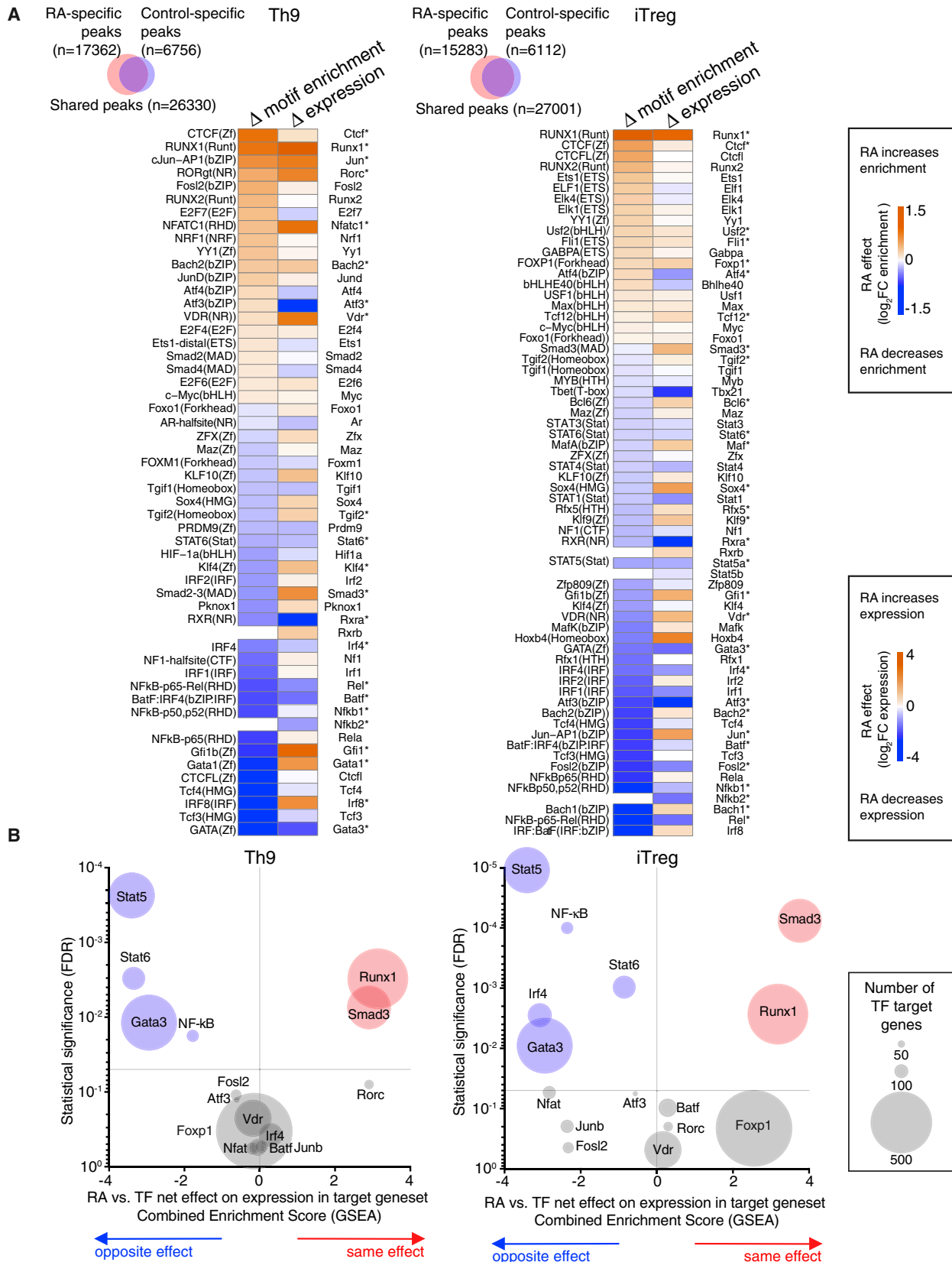


Figure 1. RA Has a Preferential Effect on the Transcriptomes of *In Vitro*-Derived Th9 and iTreg Cells

(A) The number of RA-regulated differentially expressed genes (DEGs) in different Th subsets. Isolated naïve CD4⁺ T cells were cultured with cytokines and antibodies to promote differentiation to the above Th subsets, in the presence of either vehicle control or 1,000 nM RA. After 72 h, polyadenylated mRNA was isolated and gene expression was measured by RNA-seq. Total numbers of DEGs are shown for each Th subset (fold change [FC]) in expression with RA versus vehicle control ≥ 2 or ≤ -2 , FDR < 0.05). RA regulated 191, 184, 227, 359, 444, and 534 DEGs in Th0, Th1, Th2, Th17, Th9, and iTreg cells.

(B) RA-regulated genes and pathways. RA regulated a total of 1,025 DEGs in ≥ 1 Th subset. 326 DEGs (32%) were regulated in ≥ 3 subsets, whereas 699 DEGs (68%) were regulated in ≤ 2 subsets. 428 DEGs (42%) were primarily regulated in Th9 and iTreg cells. Key pathways enriched in each group of DEGs are shown, as well as representative DEGs from each pathway (<http://metascape.org>) (Tripathi et al., 2015). (n = 2. Heatmap displays $\log_2 FC$ in expression, RA versus control; see also Figure S1.)



(legend on next page)

genes in iTreg conditions. These TFs are major positive regulators of Th9 differentiation, implying that repression of Th9 specification might be a major function of RA (Kaplan et al., 2015; Wei et al., 2011). Consistent with this, TF accessibility was reduced for PU.1; while this may be another relevant action of RA, PU.1 was expressed at very low levels ($rpk < 1$).

RA Suppresses a Th9 Transcriptional Program and Limits Th9 Differentiation

Our observation that RA opposed TFs that are important for Th9 differentiation led us to ask whether RA might impact genes differentially expressed in Th9 cells. We identified a cassette of genes differentially expressed ($FC \geq 1.5$, $FDR < 0.05$, ANOVA) in *in vitro* differentiated Th9 cells relative to other subsets (Th9-high genes, $n = 30$). Treatment with RA reduced expression of *IIL9* and other Th9-high genes (Figures 3A and 3B). Testing the overall, or net, effect of RA on this entire gene-set revealed significant downregulation (Figure S1D). RA also significantly repressed expression of genes previously identified as enriched in Th9 cells (Figure S1E) (Jabeen et al., 2013). Together, these results suggest that RA represses not only *IIL9*, but also other genes associated with a Th9 program.

To confirm the effect of RA on Th9 cells, we measured IL-9 protein under conditions used for Th9 differentiation, using Foxp3 as a control. Without RA, 30%–50% of the cultured cells produced IL-9, and 10%–30% expressed Foxp3 (Figures 3C and 3D). RA significantly reduced IL-9 production in a dose-dependent manner while increasing Foxp3 expression (Figures 3C and 3D). Under the conditions used, few Th9 cells expressed IL-10, which was repressed by RA, indicating that this was unlikely to be a mechanism by which RA repressed IL-9 (Figures S1F and S1G). Exposure to RA at later time points also inhibited IL-9 production, indicating that RA repressed IL-9 in established Th9 cells (Figures 3E and 3F). In summary, these results indicate that RA represses *IIL9* and other aspects of a Th9 transcriptional program while inducing Foxp3.

Foxp3 Is Dispensable for RA-Mediated Transcriptional Regulation of Th9 Cells

Because RA repressed Th9 differentiation while upregulating Foxp3, we expected that RA's suppressive effects would be mediated by Foxp3, which globally limits Teff function (Fontenot et al., 2003). Our ability to study the interactions between RA and Foxp3, however, was constrained by major alterations in T cell homeostasis seen in Foxp3 deficiency (Clark et al., 1999). We therefore crossed *Foxp3^{Sf}* mice that express a mutant (truncated) Foxp3 mRNA with *Rag2*-deficient, *OT-II* T cell receptor transgenic mice (*Rag2*^{−/−} *OT-II* mice; Figure S2A). The *Rag2*^{−/−}

OT-II Foxp3^{Sf} progeny failed to produce functional Foxp3 protein but preserved a population of naive CD4⁺ T cells and remained healthy (Figures S2B and S2C).

We next differentiated naive CD4⁺ cells from *Rag2*^{−/−} *OT-II* and *Rag2*^{−/−} *OT-II Foxp3^{Sf}* mice (henceforth termed *Foxp3^{WT}* and *Foxp3^{Sf}*) *in vitro* under Th9-promoting conditions. *Foxp3^{WT}* and *Foxp3^{Sf}* Th9 cells exhibited equivalent production of IL-9, indicating that Th9 differentiation was not globally dysregulated in *Foxp3^{Sf}* T cells. RA suppressed IL-9 production 3- to 4-fold in *Foxp3^{Sf}* T cells, despite the absence of functional Foxp3 (Figures 4A–4D and S2D). This effect was equivalent to that seen in *Foxp3^{WT}* T cells, establishing that RA inhibits Th9 differentiation independently of Foxp3.

We expected Foxp3 would regulate the expression of many targets besides *IIL9*, since Foxp3 was expressed in 10%–30% of *Foxp3^{WT}* cells differentiated under Th9 conditions. Yet comparing *Foxp3^{WT}* and *Foxp3^{Sf}* Th9 cells revealed no DEGs, regardless of whether the cells were differentiated in the presence or absence of RA (Figures 4E and 4F). These results led us to conclude that Foxp3 is dispensable for RA-mediated gene regulation of Th9 cells.

RA Disrupts Promoter-Enhancer Interactions of the Extended *IIL9* Locus

Because Foxp3 did not mediate RA effects on Th9 cells, we next asked whether RA directly repressed Th9 differentiation. We addressed this question by examining RA's effects on chromatin accessibility and covalent histone modifications in Th9 cells: active proximal-promoter elements (histone H3 lysine 4 trimethylation, H3K4M3), poised enhancers (H3K4 monomethylation, H3K4M1), and active enhancers (H3K27 acetylation, H3K27Ac). As a positive control, RA treatment increased H3K4M1, H3K4M3, and H3K27Ac at the extended locus of the canonical RA target gene *Ccr9*, including potential *cis*-regulatory elements (*cis*-REs) (Figure S3A).

To further dissect the link between RA-mediated chromatin remodeling, changes in gene expression, and Th9 differentiation, we examined the extended *IIL9* locus. Cell-specific accessibility was seen in the *IIL9* promoter and in three upstream REs (E1–E3; Figure S3B) (Shih et al., 2016). The most distal upstream element, E3 (previously described as SEc or CNS-25) (Koh et al., 2018; Perumal and Kaplan, 2011; Xiao et al., 2018), was broadly accessible. In contrast, E1 (previously described as CNS0 or SEb) and E2 (previously described as CNS-25 or SEc) were more accessible in Th9 cells relative to other cells. All three REs bore H3K27Ac marks (Figure 5A). RA reduced H3K4M3 at the promoter and at E1–E3, but did not change H3K4M1, indicating that the *IIL9* locus remains poised but inactive. Treatment with

Figure 2. RA Antagonizes Th9-Promoting Transcription Factors (TFs)

(A) TFs with RA-regulated motif accessibility and RA-regulated gene expression. Venn diagrams show changes in global genomic accessibility (number of ATAC peaks gained and lost) with RA treatment in Th9 and iTreg conditions. Heatmaps display RA effect on motif enrichment and gene expression for all TFs whose motif enrichment was significantly regulated by RA treatment. *FDR < 0.05.

(B) RA effect on target genes of RA-regulated TFs. Enrichment plots display a combined gene set enrichment analysis (GSEA) enrichment score and FDR for the average, or net, effect of RA on target gene sets for the following RA-regulated TFs: STAT5 (GEO: GSE77656); STAT6 (GEO: GSE22801); GATA3 (GEO: GSE20898); IRF4 (GEO: GSE39756); NF-κB (Pahl, 1999); ATF3 (GEO: GSE61055); VDR (GEO: GSE2421); FOXP1 (GEO: GSE50725); NFAT (GEO: GSE64409); JUNB (GEO: GSE98413); SMAD3 (GEO: GSE19601); RUNX1 (GEO: GSE6939); FOSL2, RORC, and BATF (GEO: GSE40918). A positive score (orange) indicates that RA has the same net effect as the TF on the target gene set, a negative score (blue) means that RA and the TF have the opposite net effect on the target gene-set, and a neutral score indicates that RA has no consistent net effect on the gene-set. The size of each data point corresponds to the size of the analyzed gene-set. For full details of analysis see *Supplemental Information*.

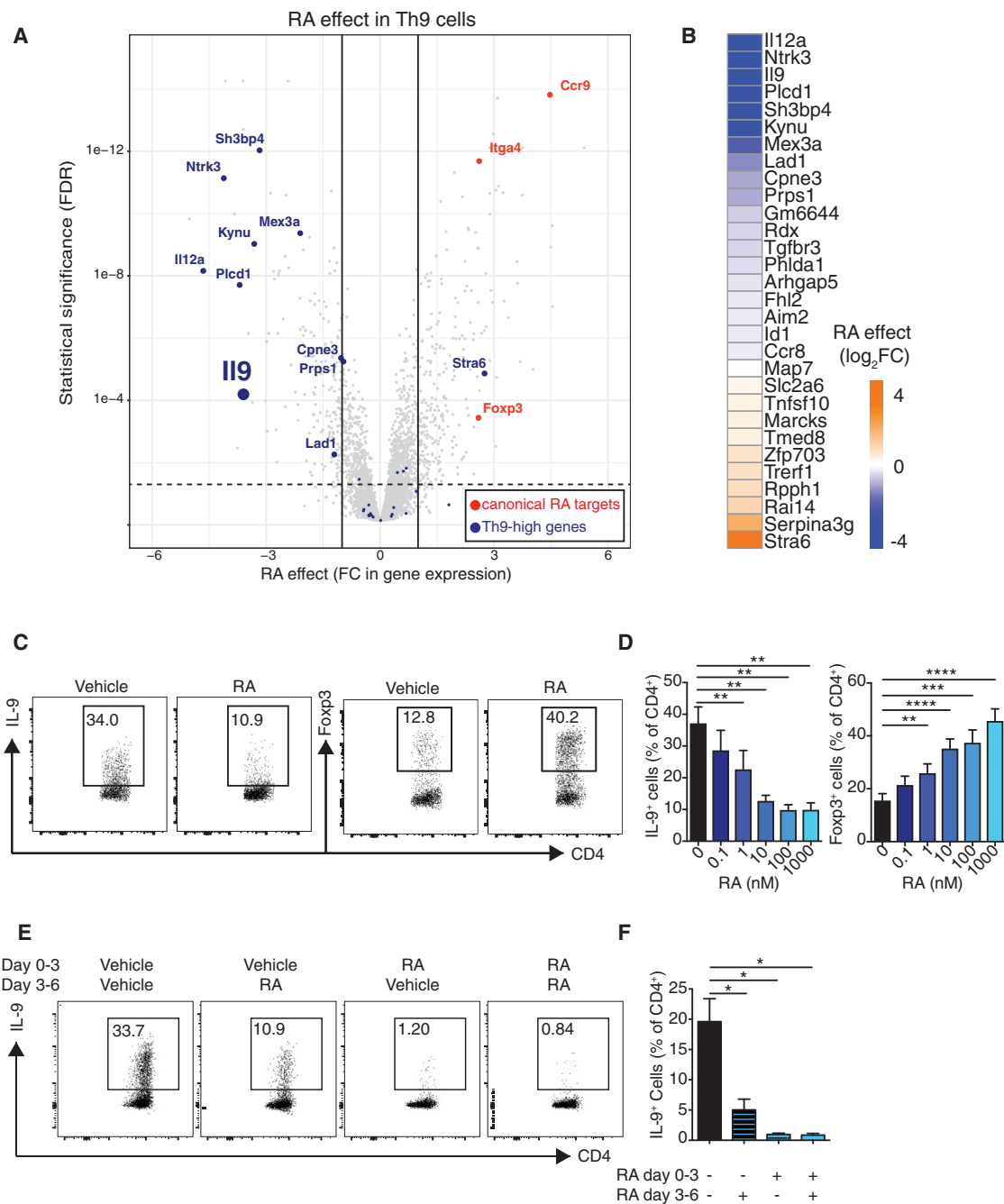
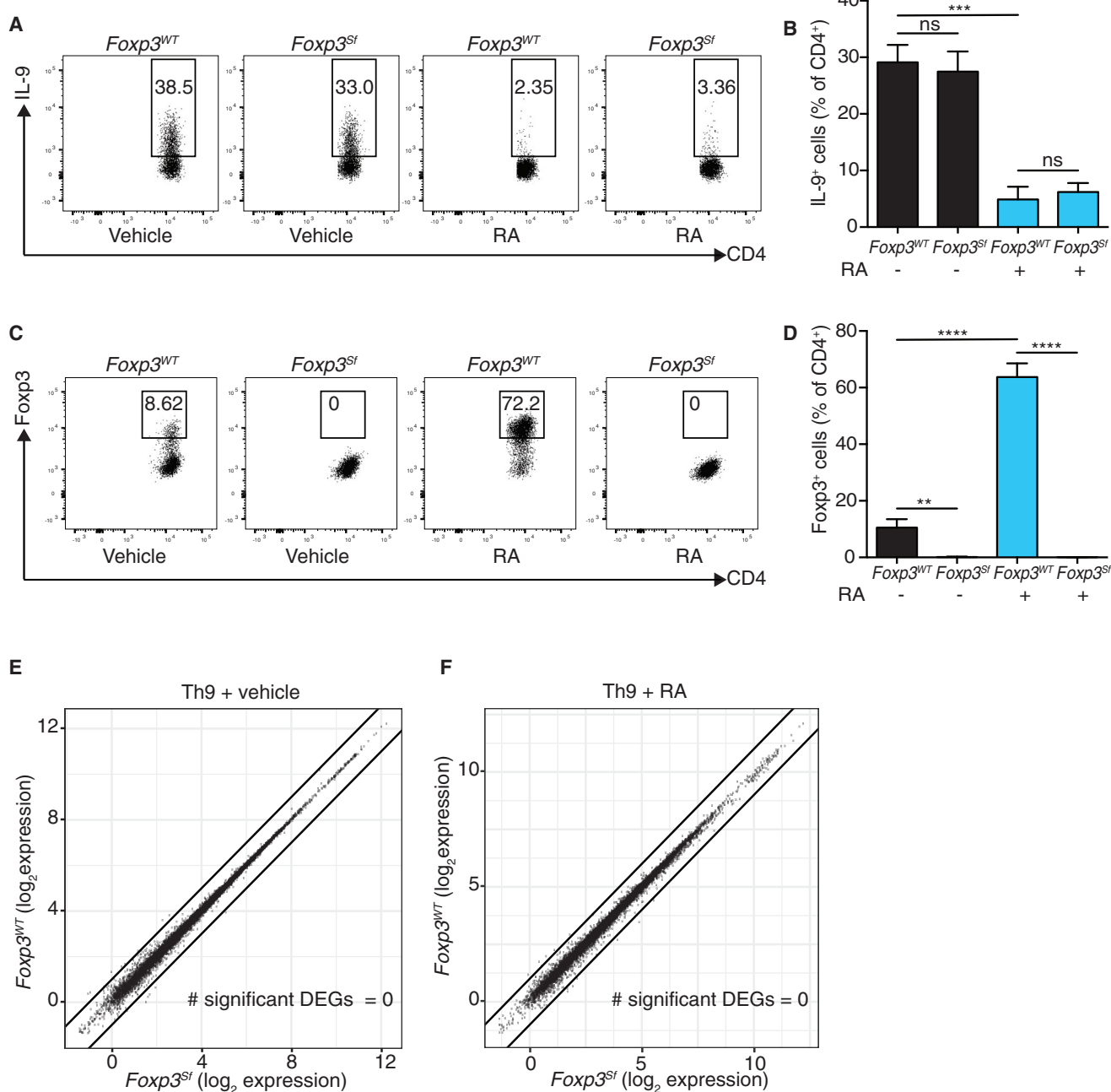


Figure 3. RA Represses a Th9 Transcriptional Program

(A) Volcano plot of gene expression in Th9 cells. Fold change in gene expression (RA versus vehicle control) versus FDR is shown for the transcriptomes of Th9 cells ($n = 2$). Selected RA-regulated genes ($FC \geq 2$ or ≤ -2 , $FDR < 0.05$) are highlighted: canonical RA-regulated genes (orange) and Th9-high genes (blue). (B) Th9-high genes and RA effect on these genes. Heatmap depicts \log_2 normalized average fold change in gene expression (RA versus vehicle control, $n = 2$) for Th9-high genes, which were selectively expressed in Th9 cells more than in Th1, Th2, Th17, and iTreg cells ($n = 30$). (C–F) Flow cytometric analysis of Th9 cells cultured in the presence of RA versus vehicle control. (C) Representative plots of IL-9 and Foxp3 expression in Th9 cells cultured with vehicle control or 1,000 nM RA. (D) Bar graph summarizing IL-9 and Foxp3 expression in Th9 cells cultured with vehicle control or escalating doses of RA ($n = 6$). (E) Representative plots of IL-9 expression in Th9 cells exposed to 1,000 nM RA at different time points. (F) Bar graph summarizing IL-9 expression ($n = 3$) (data shown as mean \pm SEM; * $p < 0.05$, ** $p < 0.01$, *** $p < 0.005$, **** $p < 0.0001$, paired t test). See also Figure S1.

RA did not change the accessibility of a downstream element (DS, previously described as CNS2 or SEA) that did not display differential cell-specific accessibility (Figure 5A).

We next determined whether E1–E3 were functional enhancers by assessing their responsiveness to STAT5. STAT5 directly regulates *Il9* expression by binding to consensus

**Figure 4. RA Acts Independently of Foxp3**

(A–D) Flow cytometric analysis of *Rag2^{-/-}* OT-II (*Foxp3^{WT}*) and *Rag2^{-/-}* OT-II *Foxp3^{Sf}* (*Foxp3^{Sf}*) cells cultured under Th9 conditions in the presence of RA versus vehicle control. (A) Representative plots of IL-9 expression in *Foxp3^{WT}* and *Foxp3^{Sf}* cells cultured with vehicle control or RA. (B) Bar graph summarizing IL-9 expression (n = 6). (C) Representative plots of Foxp3 expression in cells cultured with vehicle control or RA. (D) Bar graph summarizing Foxp3 expression (n = 6). Data shown as mean \pm SEM; **p < 0.01, ***p < 0.005, ****p < 0.0001, paired t test.

(E and F) Scatterplots comparing average gene expression in *Foxp3^{WT}* and *Foxp3^{Sf}* cells cultured under Th9 conditions, with vehicle control (E) and RA (F). Black lines indicate fold change (FC) in gene expression: ≥ 2 or ≤ -2 in *Foxp3^{WT}* versus *Foxp3^{Sf}* cells. No significant differentially expressed genes were seen (FC ≥ 2 or ≤ -2 , FDR < 0.05) [n = 2]. RA = 1,000 nM for all experiments. See also Figure S2.

sequences near the *IIL9* promoter (Liao et al., 2014), and STAT5 and STAT6 bound to E1–E3 (Figure 5A). A reporter construct containing the *IIL9* promoter element was induced 3-fold in the presence of constitutively active Stat5, whereas >2-fold

enhancer activity was seen from E1 and E2 and <1.5-fold from E3, establishing that these are STAT5-responsive enhancers (Figure S3C). We next generated mice lacking site E1 or sites E2–E3; these mice displayed no spontaneous phenotype or

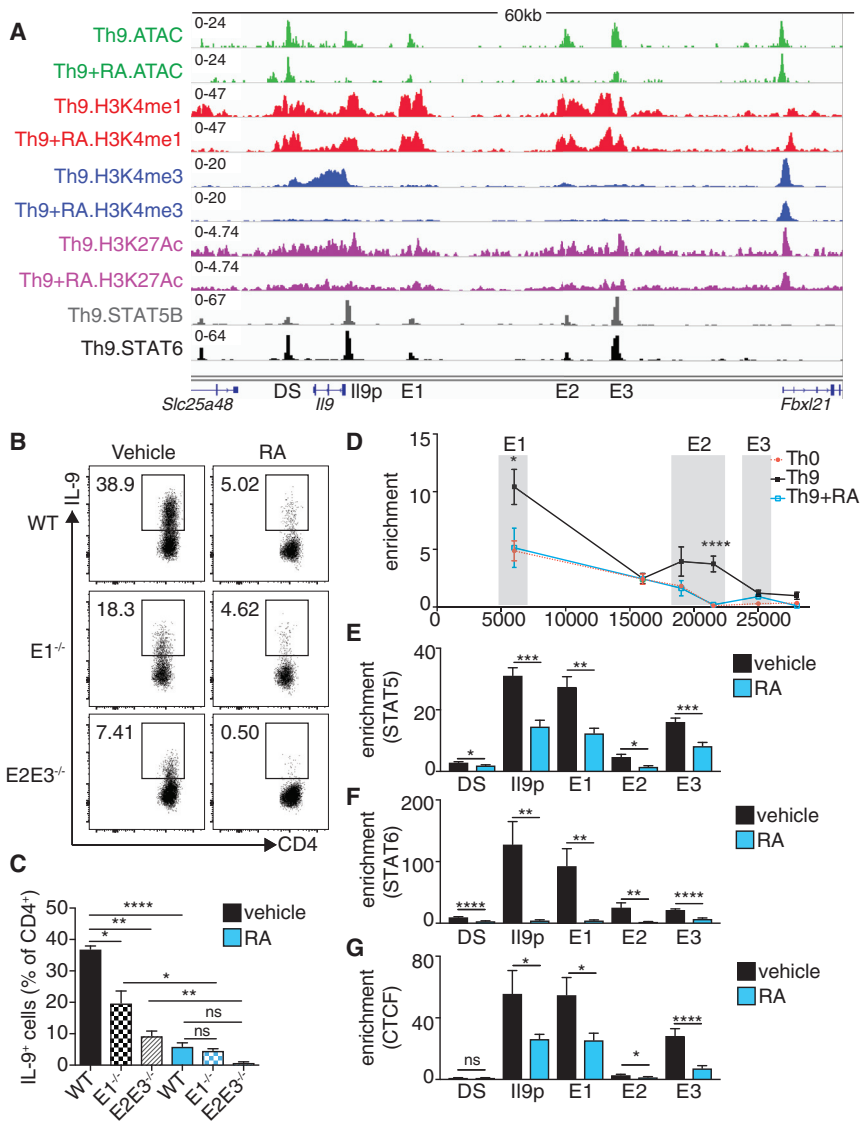


Figure 5. RA Interferes with *IL9* Promoter-Enhancer Interaction and TF Recruitment

(A) *IL9* regulatory elements (REs) identified by histone epigenetic marks and chromatin accessibility, STAT5 and STAT6 binding sites within REs, and RA effect on REs. Representative *IL9* gene tracks of ATAC, H3K4M1, H3K4M3, and H3K27Ac in Th9 cells polarized in the presence of vehicle control or RA. 5 regulatory elements are marked: the *IL9* promoter (*IL9p*), a downstream element (DS), and 3 upstream elements (E1–E3). E1–E3 and DS bear poised (H3K4M1) and active (H3K27Ac) enhancer marks, but not promoter (H3K4M3) marks (n = 2). Gene tracks also show STAT5B and STAT6 binding sites in Th9 cells based on public data (GEO: GSE41317).

(B and C) Flow cytometric analysis of IL-9 expression in Th9 cells lacking different *IL9* enhancers. (B) A 3 kb region containing E1 and an 8 kb region containing E2–E3 were deleted to generate E1^{-/-} and E2/E3^{-/-} mice, respectively. Flow cytometric plots show IL-9 expression in WT, E1^{-/-}, and E2/E3^{-/-} Th9 cells cultured with vehicle control or RA. (C) Bar graph summarizing IL-9 expression (n = 4). Data shown as mean ± SEM; *p < 0.05, **p < 0.01, ****p < 0.0001, paired t test.

(D) Activation-dependent looping of extended *IL9* locus, as measured by chromatin conformational capture (3C). Line graph depicts binding enrichment of distal regions to *IL9* promoter. For Th0 cells, enrichment decreases with increased distance from the promoter. For Th9 cells, enrichment increases for E1, decreases for an inaccessible region between E1 and E2, increases for E2, and decreases for E3. Treatment with RA reduces enrichment across the *IL9* locus. Results are significant for Th9 versus Th0 and Th9 versus Th9 + RA (n = 5).

(E–G) ChIP-qPCR for STAT5, STAT6, and CTCF at *IL9* regulatory elements in Th9 cells treated with vehicle control or RA. Bar graphs summarize binding enrichment for STAT5 (E), STAT6 (F), and CTCF (G) at the five *IL9* regulatory elements, in Th9 cells cultured with vehicle control or RA (n = 3). Pooled data shown as mean ± SEM; RA = 1,000 nM; *p < 0.05, **p < 0.01, ***p < 0.005, ****p < 0.001, unpaired t test. See also Figure S3.

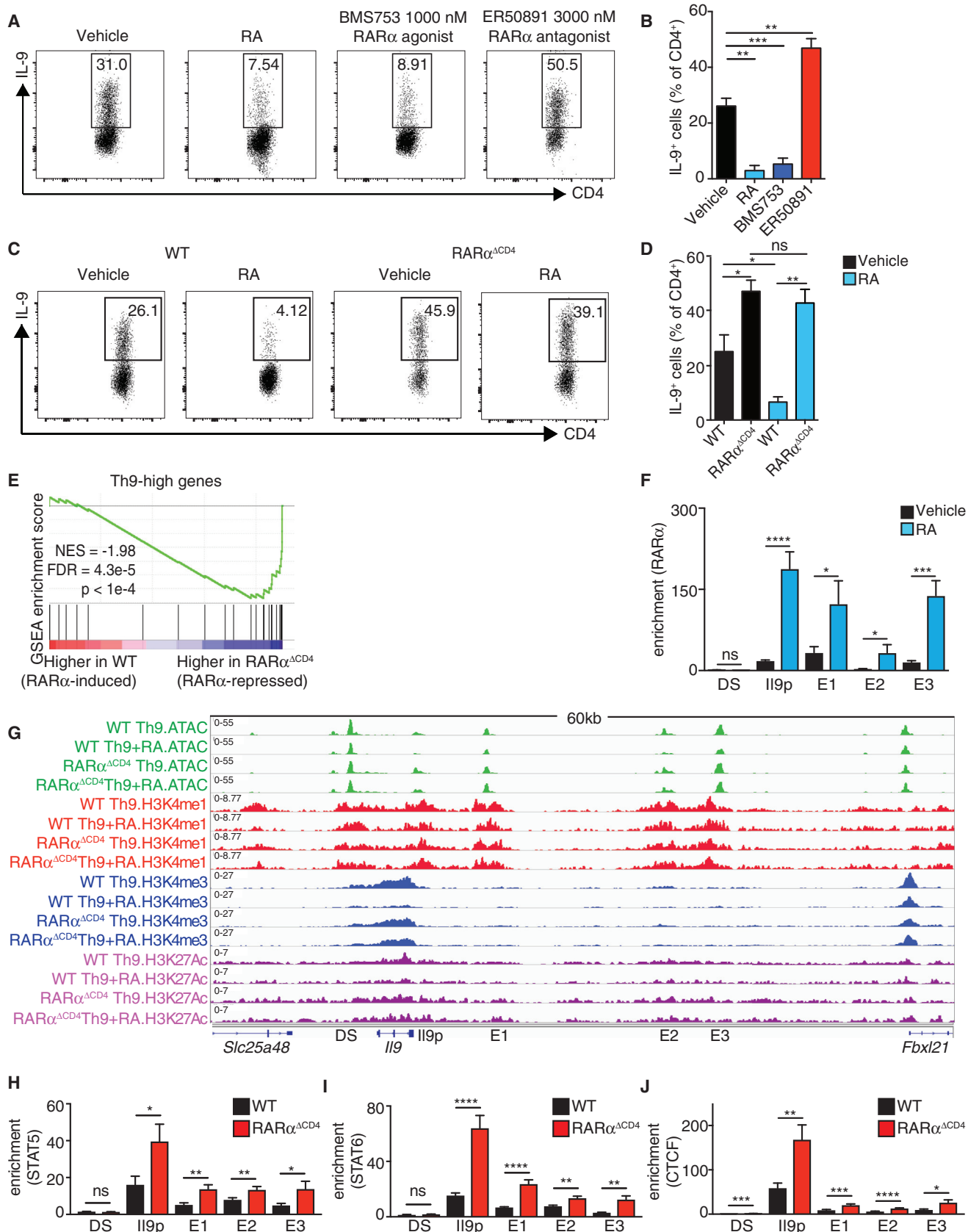
global alterations in T cell development (Figures S3D and S3E). Th9 cells generated *in vitro* from either of these lines had reduced IL-9 production, with a larger effect size from deletion of E2–E3 (Figures 5B and 5C).

To probe the mechanisms by which E1–E3 influence *IL9* transcription, we sought to determine whether these regions displayed any long-range physical interactions, or looping, with the *IL9* promoter. E1 and E2 interacted significantly with the *IL9* promoter in Th9 cells compared to nonpolarized activated T cells (Th0) (Figure 5D). Addition of RA to Th9 cultures significantly reduced E1 and E2 interaction with the *IL9* promoter, lowering it to levels similar to those in Th0 cells. CTCF, which contributes to looping between genes and distal REs, bound the *IL9* promoter and E1–E3, and RA reduced CTCF and STAT binding across the *IL9* locus (Figures 5E–5G) (Handoko et al., 2011). Thus, RA interferes with the activation of the extended *IL9* locus by reducing accessibility and disrupting normal looping.

RA-RAR α Directly Targets the Extended *IL9* Locus

To further dissect the mechanism by which RA interdicts normal function of the *IL9* locus, we next ascertained whether RAR directly regulates *IL9*. Comparing expression of different RAR isoforms revealed that Th9 cells expressed *Rara* and *Rarg*, but not *Rarb* (Figures S4A–S4C). Treating Th9 cells with a selective agonist of RAR α , the most abundant RA receptor, repressed IL-9. Conversely, treatment with a RAR α antagonist significantly increased IL-9 production (Figures 6A and 6B).

We next sought to confirm our findings using a genetic approach. We crossed mice bearing RAR α flanked by two loxP sites with mice expressing CD4-Cre to generate RAR α^{ACD4} mice. Compared to WT cells cultured under Th9 conditions, Th9 cells from RAR α^{ACD4} mice produced more IL-9 (Figures 6C and 6D). Treating RAR α -deficient T cells with RA failed to affect IL-9 levels, indicating that RAR α was a nonredundant, physiological regulator of Th9 differentiation *in vitro*.



To determine the effect of *Rara* deletion on the Th9 transcriptome and epigenome, we analyzed global changes in chromatin accessibility (ATAC-seq) and transcription (RNA-seq) in WT and RAR α -deficient Th9 cells. Deletion of RAR α increased the motif enrichment and expression of Th9-promoting TFs and increased the expression of Th9-high genes, consistent with RA-mediated repression of the Th9 program via RAR α (Figures 6E and S4D–S4F). RA induced *Foxp3* expression in RAR α -deficient Th9 cells, although less than in WT Th9 cells, indicating that alternative or redundant mechanisms underlie a portion of RA actions in Th9 cells (Figures S4G and S4H).

Having established that RA antagonized Th9 differentiation via RAR α , we next determined whether RAR α bound to *I/I9* REs. As expected, RA increased RAR α binding to a known RE associated with *Ccr9* (Figure S4I) (Ohoka et al., 2011). RA also induced binding of RAR α to the *I/I9* promoter and to E1–E3, but not to DS (Figure 6F). RA failed to reduce *I/I9*-locus accessibility or histone epigenetic marks in RAR α -deficient Th9 cells. In addition, binding of STAT5, STAT6, and CTCF increased across the locus in the absence of RAR α (Figures 6G–6J). RARs act by recruiting ligand-dependent coactivators and corepressors (le Maire and Bourguet, 2014), which in turn promote chromatin remodeling to modulate gene expression (Carroll et al., 2006; Chatagnon et al., 2015). Five ligand-dependent RAR corepressors were expressed in Th9 cells, but RA induced only one of them, *Nrip1* (Figure S4J). RA significantly increased NRIP1 binding to the promoter and to E1–E3, suggesting that RAR α recruited NRIP1 to repress *I/I9* (Figure S4K). Because RAR α would not be expected to recruit corepressors to RA-induced REs, *Ccr9* provided a useful negative control (Figure S4L).

Examining the broader impact of RAR α on the Th9 epigenome revealed that RA reduced accessibility and permissive histone marks at *cis*-REs associated with multiple Th9 genes (Figure S4M). Many of these RA-repressed loci contained STAT5 or STAT6 binding sites, consistent with our finding that RA reduced STAT5- or STAT6-binding-site accessibility. The effect of RA treatment on locus accessibility and permissive histone marks was diminished in RAR $\alpha^{\Delta CD4}$ mice. We selected two representative Th9 genes whose accessibility and permissive histone marks were repressed by RA in an RAR α -dependent manner (Figure S4N). RA increased RAR α occupancy at the promoters of these genes, suggesting that RAR α can contribute directly to the repression of genes associated with a Th9 pro-

gram (Figure S4O). In summary, RAR α not only is a nonredundant negative regulator of *I/I9* architecture and transcription but also has broader repressive effects on Th9 differentiation.

RA Ameliorates Disease in a Model of Allergic Lung Inflammation

To assess the *in vivo* relevance of our findings, we employed the chronic papain model of allergic airway inflammation (Richard et al., 2015; Sehra et al., 2015; Wilhelm et al., 2011) (Figure S5A). Mice exposed to intranasal papain developed severe peribronchial leukocyte infiltration, mucus production with airway plugging, goblet cell hyperplasia, and airway resistance. RA treatment decreased goblet cell hyperplasia, reduced peribronchial cellular infiltration, and improved airway resistance (Figures 7A–7C). In lung-resident CD4 $^{+}$ cells, treatment with RA diminished IL-9 and IL-13, but not IL-2 production (Figures 7D and S5B). RA-treated mice had fewer pulmonary Treg cells, consistent with lower overall cellular infiltration (Figure S5B). These findings confirm the *in vivo* suppressive role of RA on the type 2 allergic response, including IL-9 production, and suggest that RA-mediated suppression of type 2 immunity is independent of Tregs.

To specifically address the contribution of RA-mediated Th9 suppression, we employed an ovalbumin (Ova)-induced model of airway inflammation in which antigen-specific Th9 cells were differentiated in the presence or absence of RA and transferred into congenic hosts. To eliminate the potential contribution of *Foxp3*, we used Ova-specific Th9 cells from *Foxp3^{Sf}* mice (Figure S5C). RA inhibited IL-9 production in donor OT-II Th9 cells before and after transfer (Figures S5C–S5D), and pathology was significantly reduced in recipients of RA-treated Th9 cells (Figure S5E). These results indicate that treatment with RA reduces Th9 cell pathogenicity and that this effect is independent of *Foxp3* induction.

To determine whether endogenous RA-RAR α regulates Th9 generation and immunopathology *in vivo*, we next sensitized RAR $\alpha^{\Delta CD4}$ mice and littermate controls to intranasal papain. RAR $\alpha^{\Delta CD4}$ mice displayed more severe airway pathology and increased numbers of IL-9-producing pulmonary CD4 $^{+}$ T cells compared with WT controls, but no difference in *Foxp3* induction (Figures 7E, 7F, and S5G). Using a papain dose titrated down to avoid mucus plugging in WT mice, RAR $\alpha^{\Delta CD4}$ mice displayed heightened airway reactivity (Figures 7G and 7H). Thus,

Figure 6. RA Directly Represses IL-9 via RAR α

(A and B) Effect of RA, RAR α agonist, and RAR α antagonist on generation of Th9 cells. (A) Representative flow cytometric plots of IL-9 expression in cells cultured under Th9 conditions with vehicle control, 1,000 nM RA, 1,000 nM RAR α agonist (BMS753), or 3,000 nM RAR α antagonist (ER50891). (B) Bar graph summarizing IL-9 expression ($n = 5$).

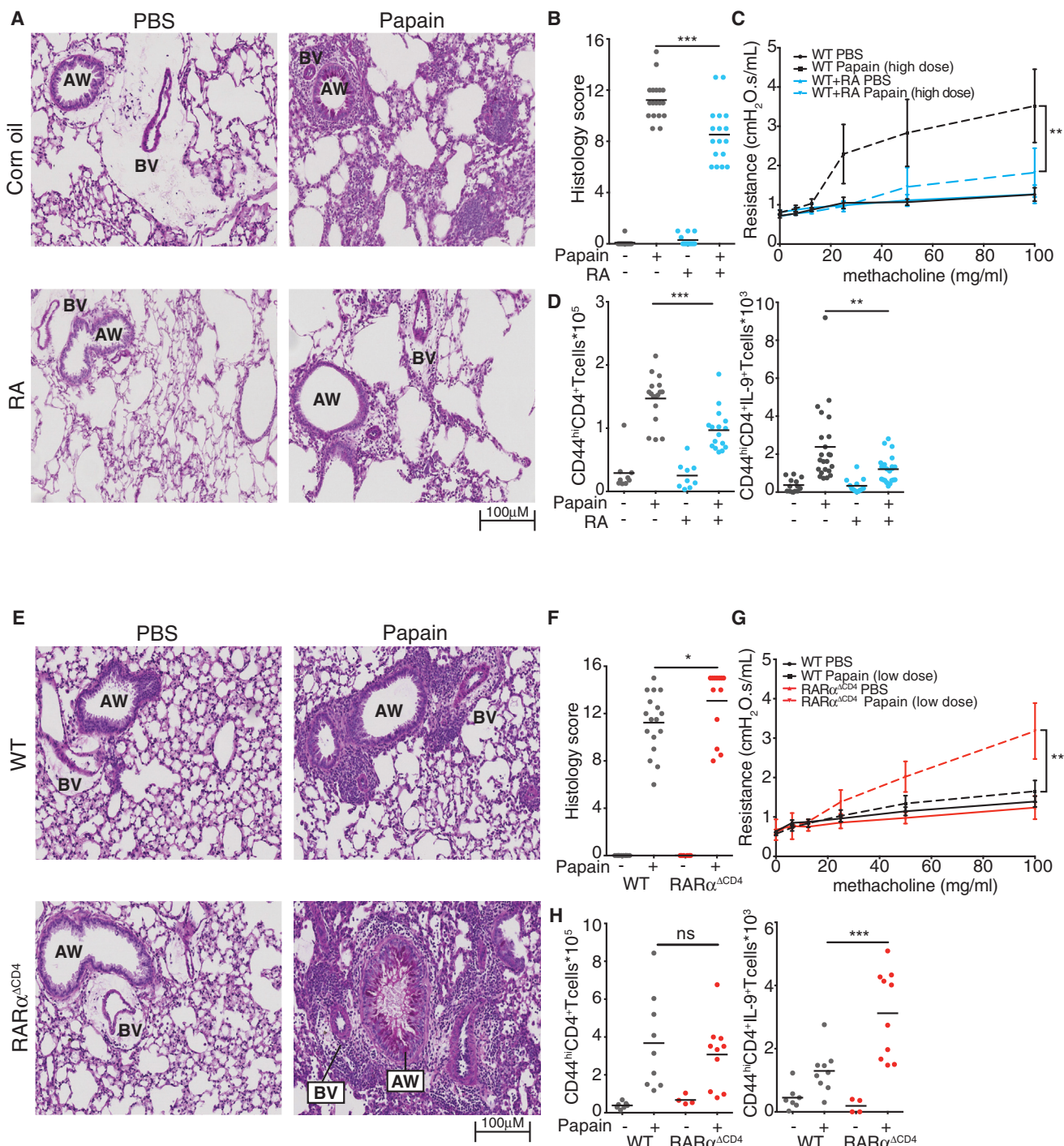
(C and D) IL-9 expression in WT versus RAR $\alpha^{\Delta CD4}$ Th9 cells. (C) Representative flow cytometric plots of IL-9 expression in cells cultured under Th9 conditions with vehicle control or 1,000 nM RA. (D) Bar graph summarizing IL-9 expression ($n = 5$). Flow data shown as mean \pm SEM; * $p < 0.05$, ** $p < 0.01$, *** $p < 0.005$, **** $p < 0.001$, paired t test.

(E) RAR α suppresses net expression of Th9-high genes. GSEA plot depicts the effect of RAR α deletion on Th9-high genes, accounting for the net, or average, effect on all the genes in the gene set.

(F) ChIP-qPCR for RAR α at *I/I9* regulatory elements in Th9 cells treated with vehicle control or RA. Bar graphs summarize binding enrichment for RAR α relative to input at the five *I/I9* regulatory elements ($n = 3$).

(G) RA effect on histone modifications and accessibility of *I/I9* regulatory elements (REs) in WT versus RAR $\alpha^{\Delta CD4}$ Th9 cells polarized in the presence of vehicle control or RA. ($n = 2$ –4).

(H–J) ChIP-qPCR for STAT5, STAT6, and CTCF at *I/I9* regulatory elements in WT or RAR $\alpha^{\Delta CD4}$ Th9 cells. Bar graphs summarize binding enrichment for STAT5 (H), STAT6 (I), and CTCF (J) at the five *I/I9* regulatory elements, in WT or RAR $\alpha^{\Delta CD4}$ Th9 cells ($n = 3$ –5); ChIP-qPCR data shown as mean \pm SEM; * $p < 0.05$, ** $p < 0.01$, *** $p < 0.005$, **** $p < 0.001$, unpaired t test. See also Figure S4.

**Figure 7. RA Is Essential to Control Pathology in Allergic Lung Disease**

(A–C) RA effect on lung inflammation and airway resistance. (A) Representative images of periodic acid-Schiff (PAS)-stained lung tissue demonstrate reduced mucus production and lymphocytic infiltration in RA-treated versus vehicle-treated mice with papain-induced asthma. (B) Pulmonary histology scores in mice treated with RA and vehicle (3 replicates, n = 3–6 per replicate). (C) Airway resistance in mice exposed to escalating doses of intratracheal methacholine to induce bronchospasm. 2 replicates, n = 1–3 per replicate.

(D) Flow cytometric analysis of IL-9 producing T cells in lung tissue at day 14 (d14) of papain-induced asthma. Graphs show total numbers of Lin⁻TCR β^+ CD4⁺CD44^{hi} cells and of IL-9⁺ Lin⁻TCR β^+ CD4⁺CD44^{hi} T cells extracted from lung tissue of mice treated with vehicle control or RA. 4 replicates, n = 3–5 per replicate.

(E–G) Lung inflammation and airway resistance in WT and RAR α^{ACD4} mice at d14 of papain-induced asthma. (E) Representative images of PAS-stained slides demonstrate increased lymphocytic infiltration in RAR α^{ACD4} versus WT mice. (F) Pulmonary histology scores in WT and RAR α^{ACD4} mice. (3 replicates, n = 3–5 per replicate)

(legend continued on next page)

physiologic RAR α signaling in CD4 $^+$ T cells was highly relevant for *in vivo* Th9 specification and allergic pathology.

RA-RAR α Signaling Suppresses a Shared *In Vitro* and *In Vivo* Th9 Transcriptional Program

The finding that RA ameliorated Th9 pathology *in vivo* led us to hypothesize that RA-RAR α suppressed transcriptional programs of *in vivo* IL-9-producing cells. To this end, we identified genes expressed by IL-9-producing T cells using two different IL-9 reporter mice (GFP $^+$ and eYFP $^+$) challenged with papain (Licona-Límon et al., 2013; Richard et al., 2015; Sehra et al., 2015) (Figures S6A and S6B). We noted substantial differences between the genes expressed in IL-9-producing cells identified by the two different reporters and therefore compiled DEGs in at least one reporter model (Figures S6C–S6D). In addition to *IIL9* and other genes associated with Th9 differentiation (*Spi1*, *IIL17rb*, *Ccl17*), this cassette also included a number of Th2 (*IIL4*, *IIL13*, *Gata3*) and Th17 (*Ccl3*, *Lag3*, *Csf2*) signature genes (Hu et al., 2017; Humblin et al., 2017; Li et al., 2013; Perumal and Kaplan, 2011). We therefore excluded genes expressed by alternative fates by determining the intersection with genes preferentially expressed by *in vitro* differentiated Th9 cells relative to other subsets (average FC \geq 1.5, FDR $<$ 0.05, ANOVA). Using these criteria, a cassette of 62 genes was designated as “shared Th9” (Figure S6E). Treatment with RA reduced expression of shared Th9 genes, whereas deletion of RAR α increased expression of these genes (Figures S6F–S6I). Taken together, these findings indicate that RA and RAR α broadly repress a transcriptomic program in Th9 cells, recognizing that this is a heterogeneous group.

RA-RAR Signaling Is Aberrant in Human Th9-Associated Disease

The finding that RA-RAR signaling repressed *in vivo* Th9 genes and improved Th9-associated immunopathology led us to question whether RA signaling had a role in human Th9-associated inflammation. RA inhibited human Th9 differentiation, similar to its effects in mice (Figures S7A and S7B). RA target genes (Figure 1B) were also dysregulated in skin from nickel-allergic patients and in CD4 $^+$ T cells from atopic individuals stimulated *in vitro* with house dust mite extract (Pedersen et al., 2007; Troy et al., 2016). House dust mite stimulation was associated with decreased expression of RA-induced genes and increased expression of RA-repressed genes, including increased *IL9* and *IL13* expression (Figures S7C–S7E). Nickel exposure was similarly associated with increased expression of RA-repressed genes, including *IL9* (Figures S7F–S7H). Expression of *NRIP1* and RA-metabolizing enzymes was lower in nickel-allergic skin than in healthy skin. Conversely, expression of the retinaldehyde-reducing enzyme *DHRS3* was higher in allergic skin (Figures S7I and S7J). These results suggest that allergic inflammation in humans is associated with reduced RA signaling, indicating potential translational relevance.

DISCUSSION

Vitamin A and its metabolite RA have long been identified as key immunomodulators, yet a number of issues remain unclear, including the comprehensive effect of RA across T effector subsets, the role of Foxp3 in mediating RA signaling, and the direct effects of RAR in Th9 cells that reside in RA-rich mucosal environments. Herein, we addressed these questions using genomic and functional approaches, revealing molecular mechanisms underlying RA actions in Th9 cell specification and function *in vitro* and *in vivo*.

RA antagonized Th9-promoting TFs and repressed a broader Th9 transcriptional program indicating a major role for RA signaling in this Th subset. Vitamin A deficiency is associated with increased prevalence and severity of asthma (Arora et al., 2002; Marquez and Cardoso, 2016), and our analysis suggests that RA signaling is reduced in the setting of acute allergic inflammation. Moreover, RA triggered chromatin remodeling across the *IIL9* locus and at the loci of other Th9 genes via RAR α . While direct RAR α binding was shown at selected Th9 genes, we were unable to obtain reliable RAR α chromatin immunoprecipitation sequencing (ChIP-sequencing) data. Improved reagents with more specificity could conclusively document genome-wide RAR α binding and establish a direct mechanism for the broader Th9 program. Critically, Th9 differentiation was repressed across a range of doses and under a range of physiologic conditions, as RAR α -deficient Th9 cells differentiated more efficiently and mediated more severe lung disease. This distinguishes our work from previous studies in which low concentrations of RA have been found essential for a productive immune response (Brown et al., 2015; Hall et al., 2011a; Iwata et al., 2003).

Our findings also advance the understanding of how the *IIL9* locus is dynamically regulated, which is important because the factors governing Th9 differentiation and function are incompletely characterized (Kaplan et al., 2015). Th9 cells are regulated by a network of TF modules including cytokine-dependent TFs (STATs, Smad/RBP-J κ /Notch, TAK1), antigen receptor-dependent TFs (BATF/IRF4, NFAT/NFKB), and lineage-determining TFs (ETV5/PU.1) (Kaplan, 2017). RAR α can now be added to this network as a metabolite-dependent TF, distinguishing it from other Th9-regulating signals. Moreover, the characterization of enhancers within the extended *IIL9* locus may provide insight into the actions of other Th9-promoting TFs. For example, enhancer DS is more relevant to the activity of OX40 and RelB than are E1–E3, whereas E1–E3 were important for STAT5-dependent IL-9 production (Koh et al., 2018; Xiao et al., 2018).

Aside from its effect on the *IIL9* locus, RA had a broad impact on chromatin status and transcriptomes of IL-9-producing cells. Analysis of *in vivo* Th9 cells revealed a core set of genes highly expressed in both *in vitro* differentiated and *in vivo* Th9 cells. Nonetheless, substantial differences existed between *in vitro* and *in vivo* Th9 cells and between the two different reporter models of IL-9 *in vivo*. The reasons for these differences are

per replicate.) (G) Airway resistance in mice exposed to escalating doses of intratracheal methacholine to induce bronchospasm. 3 replicates, n = 1–3 per experiment.

(H) Flow cytometric analysis of IL-9-producing T cells in lung tissue at d14 of papain-induced asthma. Graphs show total numbers of Lin $^-$ TCR β^+ CD4 $^+$ CD44 hi cells and of IL-9 $^-$ Lin $^-$ TCR β^+ CD4 $^+$ CD44 hi T cells extracted from lung tissue of WT and RAR α^{ACD4} mice (2 replicates, n = 3–5 per replicate). *p < 0.05, **p < 0.01, ***p < 0.005, Mann-Whitney; AW, Airway; BV, blood vessel. See also Figures S5–S7.

unclear, but IL-9-producing cells apparently represent a heterogeneous collection, and there is much to learn about exactly what a Th9 cell is (Malik and Awasthi, 2018). A comprehensive and dynamic understanding of IL-9-producing Th cells and their relationship to other subsets will require further investigation and methodologies, including multi-cytokine reporter mice and dual reporter or fate reporter models. These insights will clarify the identity and functionality of IL-9-producing cells in the context of not only type 2 immunity but also inflammatory bowel disease and antitumor immunity, where Th9 cells are implicated in disease pathogenesis.

Although RA strongly induced Foxp3, which profoundly limits T effector function, Foxp3 was unexpectedly dispensable for RA-mediated regulation of the Th9 transcriptome. Instead, RAR α directly targeted the *IIL9* locus by recruiting the corepressor NRIP1 and reducing chromatin accessibility. RA-mediated chromatin remodeling interfered with TFs that promoted *IIL9* transcription and prevented binding of CTCF, blocking promoter-enhancer looping. These results address a major gap in retinoid biology, as the regulation and function of RA-dependent coregulators in CD4 $^{+}$ T cells has not been described (Larange and Cheroutre, 2016).

Although vitamin A can also enhance type 2 immunity (Schuster et al., 2008), the discrepancy with our findings could be due to the existence of several mechanistically distinct vitamin A-driven regulatory networks. RA-RAR α signaling repressed Th9 differentiation, but retinoid X receptor (RXR) ligands may enhance the production of cytokines such as IL-5, which are more important for some models of airway disease (Stephensen et al., 2002). Retinoids also regulate respiratory epithelial cells and can indirectly regulate Th-driven immune responses by priming dendritic cells, which activate Th cells (Maret et al., 2007; Rampal et al., 2016). It will be critical to consider these and other potentially competing mechanisms, including the effects of RA on other cell types, in elucidating the immunomodulatory effects of vitamin A and its metabolites. Future investigations exploring the specific role of RAR α using genetic models should address these questions.

By systematically characterizing RA-regulated genes in all major *in vitro*-generated Th subsets, our findings can also be used to explain some of the paradoxical effects of RA. For example, RA repressed a cassette of genes in iTreg and Th9 cells but induced the same cassette in Th17 cells. This could be because RARs work cooperatively with cofactors; the cell-specific expression of a particular cofactor could determine the directionality of RA's effect on a specific gene in that cell type. Dissecting the mechanisms by which divergent regulation occurs in different subsets will be an interesting area for future investigation. RA also had divergent impacts on various Th17-promoting genes, repressing *IIL6ra* while inducing *Runx1*. Such findings help explain the ostensibly contradictory effects of RA in Th17 specification, although confirmation will require *in vivo* models and genetic tools (Takahashi et al., 2012).

In summary, RA signaling had a major effect in Th9 cells that involved suppression of the Th9 transcriptional program, independently of Foxp3 induction. RAR α suppressed the global Th9 epigenome and targeted three functional enhancers within the extended *IIL9* locus. Finally, RA signaling was aberrant in the setting of Th9-associated human inflammation. These results

advance the field of Th9 biology, which is becoming increasingly relevant as new roles emerge for Th9 cells in the pathogenesis of human disease.

STAR★METHODS

Detailed methods are provided in the online version of this paper and include the following:

- **KEY RESOURCES TABLE**
- **CONTACT FOR REAGENT AND RESOURCE SHARING**
- **EXPERIMENTAL MODEL AND SUBJECT DETAILS**
- **METHOD DETAILS**
 - Generation of Enhancer Knockout Mice
 - Media
 - Reagents
 - Cell Culture
 - Flow Cytometry
 - RNA-seq
 - ATAC-seq
 - Histone Chromatin Immunoprecipitation and ChIP-seq
 - Sonication: Histone Chromatin Immunoprecipitation
 - Transcription Factor Chromatin Immunoprecipitation and ChIP-qPCR
 - Immunoprecipitation, Library Preparation, and ChIP-qPCR
 - Cell Lines and Transfection
 - Luciferase Detection
 - Chromatin Conformational Capture (3C)
 - Papain Induced Asthma
 - Th9 Transfer Experiment
 - Measurement of Allergic Airway Reactivity
- **QUANTIFICATION AND STATISTICAL ANALYSIS**
 - RNA-seq Analysis
 - Cell-Specific and Shared RA-Regulated Modules
 - Evaluation of Functional Enrichment
 - Gene Sensitivity Enrichment Analysis
 - Selection and Analysis of Human Datasets
 - ChIP-seq Alignment and Peak Calling
 - ATAC-seq Alignment and Peak Calling
 - Analysis of ATAC-seq and ChIP-seq Peaks
 - Statistical Analysis of RNA-seq, qPCR, Flow Cytometry, and *In Vivo* Experiments
 - Scoring: Papain- and Ova-Induced Asthma
- **DATA AND SOFTWARE AVAILABILITY**

SUPPLEMENTAL INFORMATION

Supplemental Information includes seven figures and three tables and can be found with this article online at <https://doi.org/10.1016/j.immuni.2018.12.014>.

ACKNOWLEDGMENTS

We thank J. Simone, J. Lay, and K. Tinsley (NIAMS) for expert assistance in flow cytometry and the NIAMS LACU staff for technical support. We thank C. Liu and F. Zhang (NHLBI) for generating knockout mouse lines. We thank G. Gutierrez-Cruz and S. Dell'Orso (NIAMS) for deep-sequencing support. This study utilized the high-performance computational capabilities of the Biowulf Linux cluster (NIH). This work was supported by the Intramural Research Programs of NIAMS and NIAID, and by the Office of Dietary Supplements (ODS).

AUTHOR CONTRIBUTIONS

Conceptualization, D.S., A.L., J.O'S.; Methodology, D.S., F.M.; Software, D.S., H.-W.S., H.Y.S., F.P.D.; Validation, D.S., F.M.; Formal Analysis, D.S., H.-W.S.; Investigation, D.S., T.F., N.R., H.Y.S., F.P., Y.M., E.H., K.J., C.Y., Y.Z.; Writing, D.S., Y.K., F.P.D., and J.O'S.; Visualization, D.S.; Supervision, F.M., A.L., J.O'S., J.M.; Funding Acquisition, D.S., R.S., and J.O'S.

DECLARATION OF INTERESTS

The authors declare no competing interests.

Received: November 1, 2017

Revised: September 20, 2018

Accepted: December 12, 2018

Published: January 15, 2019

REFERENCES

- Abbas, A.K., Murphy, K.M., and Sher, A. (1996). Functional diversity of helper T lymphocytes. *Nature* 383, 787–793.
- Arora, P., Kumar, V., and Batra, S. (2002). Vitamin A status in children with asthma. *Pediatr. Allergy Immunol.* 13, 223–226.
- Bai, X.F., Li, O., Zhou, Q., Zhang, H., Joshi, P.S., Zheng, X., Liu, Y., Wang, Y., Zheng, P., and Liu, Y. (2004). CD24 controls expansion and persistence of autoreactive T cells in the central nervous system during experimental autoimmune encephalomyelitis. *J. Exp. Med.* 200, 447–458.
- Benson, M.J., Pino-Lagos, K., Rosemblatt, M., and Noelle, R.J. (2007). All-trans retinoic acid mediates enhanced T reg cell growth, differentiation, and gut homing in the face of high levels of co-stimulation. *J. Exp. Med.* 204, 1765–1774.
- Brown, C.C., Esterhazy, D., Sarde, A., London, M., Pullabhatla, V., Osma-Garcia, I., Al-Bader, R., Ortiz, C., Elgueta, R., Arno, M., et al. (2015). Retinoic acid is essential for Th1 cell lineage stability and prevents transition to a Th17 cell program. *Immunity* 42, 499–511.
- Buenrostro, J.D., Giresi, P.G., Zaba, L.C., Chang, H.Y., and Greenleaf, W.J. (2013). Transposition of native chromatin for fast and sensitive epigenomic profiling of open chromatin, DNA-binding proteins and nucleosome position. *Nat. Methods* 10, 1213–1218.
- Carroll, J.S., Meyer, C.A., Song, J., Li, W., Geistlinger, T.R., Eeckhoute, J., Brodsky, A.S., Keeton, E.K., Fertuck, K.C., Hall, G.F., et al. (2006). Genome-wide analysis of estrogen receptor binding sites. *Nat. Genet.* 38, 1289–1297.
- Chatagnon, A., Veber, P., Morin, V., Bedo, J., Triqueneaux, G., Sémon, M., Laudet, V., d'Alché-Buc, F., and Benoit, G. (2015). RAR/RXR binding dynamics distinguish pluripotency from differentiation associated cis-regulatory elements. *Nucleic Acids Res.* 43, 4833–4854.
- Clark, L.B., Appleby, M.W., Brunkow, M.E., Wilkinson, J.E., Ziegler, S.F., and Ramsdell, F. (1999). Cellular and molecular characterization of the scurfy mouse mutant. *Journal of Immunol.* 162, 2546–2554.
- Coombes, J.L., Siddiqui, K.R., Arancibia-Cárcamo, C.V., Hall, J., Sun, C.M., Belkaid, Y., and Powrie, F. (2007). A functionally specialized population of mucosal CD103+ DCs induces Foxp3+ regulatory T cells via a TGF-beta and retinoic acid-dependent mechanism. *J. Exp. Med.* 204, 1757–1764.
- Dong, C., and Flavell, R.A. (2000). Control of T helper cell differentiation—in search of master genes. *Sci. STKE* 2000, pe1.
- Dong, C., Juedes, A.E., Temann, U.A., Shresta, S., Allison, J.P., Ruddle, N.H., and Flavell, R.A. (2001). ICOS co-stimulatory receptor is essential for T-cell activation and function. *Nature* 409, 97–101.
- Elias, K.M., Laurence, A., Davidson, T.S., Stephens, G., Kanno, Y., Shevach, E.M., and O'Shea, J.J. (2008). Retinoic acid inhibits Th17 polarization and enhances FoxP3 expression through a Stat-3/Stat-5 independent signaling pathway. *Blood* 111, 1013–1020.
- Fontenot, J.D., Gavin, M.A., and Rudensky, A.Y. (2003). Foxp3 programs the development and function of CD4+CD25+ regulatory T cells. *Nat. Immunol.* 4, 330–336.
- Hall, J.A., Cannons, J.L., Grainger, J.R., Dos Santos, L.M., Hand, T.W., Naik, S., Wohlfert, E.A., Chou, D.B., Oldenhove, G., Robinson, M., et al. (2011a). Essential role for retinoic acid in the promotion of CD4(+) T cell effector responses via retinoic acid receptor alpha. *Immunity* 34, 435–447.
- Hall, J.A., Grainger, J.R., Spencer, S.P., and Belkaid, Y. (2011b). The role of retinoic acid in tolerance and immunity. *Immunity* 35, 13–22.
- Handoko, L., Xu, H., Li, G., Ngan, C.Y., Chew, E., Schnapp, M., Lee, C.W., Ye, C., Ping, J.L., Mulawadi, F., et al. (2011). CTCF-mediated functional chromatin interactome in pluripotent cells. *Nat. Genet.* 43, 630–638.
- Hu, D., Notarbartolo, S., Croonenborghs, T., Patel, B., Cialic, R., Yang, T.H., Aschenbrenner, D., Andersson, K.M., Gattorno, M., Pham, M., et al. (2017). Transcriptional signature of human pro-inflammatory T_H17 cells identifies reduced IL10 gene expression in multiple sclerosis. *Nat. Commun.* 8, 1600.
- Humblin, E., Thibaudin, M., Chalmin, F., Derangère, V., Limagne, E., Richard, C., Flavell, R.A., Chevrier, S., Ladoire, S., Berger, H., et al. (2017). IRF8-dependent molecular complexes control the Th9 transcriptional program. *Nat. Commun.* 8, 2085.
- Iwata, M., Eshima, Y., and Kagechika, H. (2003). Retinoic acids exert direct effects on T cells to suppress Th1 development and enhance Th2 development via retinoic acid receptors. *Int. Immunopharmacol.* 15, 1017–1025.
- Iwata, M., Hirakiyama, A., Eshima, Y., Kagechika, H., Kato, C., and Song, S.Y. (2004). Retinoic acid imprints gut-homing specificity on T cells. *Immunity* 21, 527–538.
- Jabeen, R., Goswami, R., Awe, O., Kulkarni, A., Nguyen, E.T., Attenasio, A., Walsh, D., Olson, M.R., Kim, M.H., Tepper, R.S., et al. (2013). Th9 cell development requires a BATF-regulated transcriptional network. *J. Clin. Invest.* 123, 4641–4653.
- Josefowicz, S.Z., and Rudensky, A. (2009). Control of regulatory T cell lineage commitment and maintenance. *Immunity* 30, 616–625.
- Kaplan, M.H. (2017). The transcription factor network in Th9 cells. *Semin. Immunopathol.* 39, 11–20.
- Kaplan, M.H., Hufford, M.M., and Olson, M.R. (2015). The development and in vivo function of T helper 9 cells. *Nat. Rev. Immunol.* 15, 295–307.
- Koh, B., Abdul Qayum, A., Srivastava, R., Fu, Y., Ulrich, B.J., Janga, S.C., and Kaplan, M.H. (2018). A conserved enhancer regulates IL9 expression in multiple lineages. *Nat. Commun.* 9, 4803.
- Kwok, S.K., Park, M.K., Cho, M.L., Oh, H.J., Park, E.M., Lee, D.G., Lee, J., Kim, H.Y., and Park, S.H. (2012). Retinoic acid attenuates rheumatoid inflammation in mice. *Journal of Immunol.* 189, 1062–1071.
- Larange, A., and Cheroutre, H. (2016). Retinoic Acid and Retinoic Acid Receptors as Pleiotropic Modulators of the Immune System. *Annu. Rev. Immunol.* 34, 369–394.
- Le Maire, A., and Bourguet, W. (2014). Retinoic acid receptors: structural basis for coregulator interaction and exchange. *Subcell. Biochem.* 70, 37–54.
- Lee, W., Su Kim, H., and Lee, G.R. (2015). Leukotrienes induce the migration of Th17 cells. *Immunol. Cell Biol.* 93, 472–479.
- Li, H., Edin, M.L., Bradbury, J.A., Graves, J.P., DeGraff, L.M., Gruzdev, A., Cheng, J., Dackor, R.T., Wang, P.M., Bortner, C.D., et al. (2013). Cyclooxygenase-2 inhibits T helper cell type 9 differentiation during allergic lung inflammation via down-regulation of IL-17RB. *Am. J. Respir. Crit. Care Med.* 187, 812–822.
- Liao, W., Spolski, R., Li, P., Du, N., West, E.E., Ren, M., Mitra, S., and Leonard, W.J. (2014). Opposing actions of IL-2 and IL-21 on Th9 differentiation correlate with their differential regulation of BCL6 expression. *Proc. Natl. Acad. Sci. USA* 111, 3508–3513.
- Licona-Limón, P., Henao-Mejía, J., Temann, A.U., Gagliani, N., Licona-Limón, I., Ishigame, H., Hao, L., Herbert, D.R., and Flavell, R.A. (2013). Th9 Cells Drive Host Immunity against Gastrointestinal Worm Infection. *Immunity* 39, 744–757.
- Malik, S., and Awasthi, A. (2018). Transcriptional Control of Th9 Cells: Role of Foxo1 in Interleukin-9 Induction. *Front. Immunol.* 9, 995.
- Manicassamy, S., Ravindran, R., Deng, J., Oluoch, H., Denning, T.L., Kasturi, S.P., Rosenthal, K.M., Evavold, B.D., and Pulendran, B. (2009). Toll-like receptor 2-dependent induction of vitamin A-metabolizing enzymes in dendritic cells

- promotes T regulatory responses and inhibits autoimmunity. *Nat. Med.* **15**, 401–409.
- Maret, M., Ruffie, C., Periquet, B., Campo, A.M., Menevret, M., Phelep, A., Dziewiszek, K., Druilhe, A., and Pretolani, M. (2007). Liposomal retinoic acids modulate asthma manifestations in mice. *J. Nutr.* **137**, 2730–2736.
- Marquez, H.A., and Cardoso, W.V. (2016). Vitamin A-retinoid signaling in pulmonary development and disease. *Molecular and Cellular Pediatrics* **3**, 28.
- Maynard, C.L., Hatton, R.D., Helms, W.S., Oliver, J.R., Stephensen, C.B., and Weaver, C.T. (2009). Contrasting roles for all-trans retinoic acid in TGF-beta-mediated induction of Foxp3 and IL10 genes in developing regulatory T cells. *J. Exp. Med.* **206**, 343–357.
- Meyer Zu Horste, G., Wu, C., Wang, C., Cong, L., Pawlak, M., Lee, Y., Elyaman, W., Xiao, S., Regev, A., and Kuchroo, V.K. (2016). RBPJ Controls Development of Pathogenic Th17 Cells by Regulating IL-23 Receptor Expression. *Cell Rep.* **16**, 392–404.
- Miossec, P., Korn, T., and Kuchroo, V.K. (2009). Interleukin-17 and type 17 helper T cells. *N. Engl. J. Med.* **361**, 888–898.
- Mizutani, N., Nabe, T., and Yoshino, S. (2015). Semaphorin 7A plays a critical role in IgE-mediated airway inflammation in mice. *Eur. J. Pharmacol.* **764**, 149–156.
- Moisan, J., Grenningloh, R., Bettelli, E., Oukka, M., and Ho, I.C. (2007). Ets-1 is a negative regulator of Th17 differentiation. *J. Exp. Med.* **204**, 2825–2835.
- Mucida, D., Park, Y., Kim, G., Turovskaya, O., Scott, I., Kronenberg, M., and Cheroutre, H. (2007). Reciprocal TH17 and regulatory T cell differentiation mediated by retinoic acid. *Science* **317**, 256–260.
- Naus, S., Blanchet, M.R., Gossens, K., Zaph, C., Bartsch, J.W., McNagny, K.M., and Ziltener, H.J. (2010). The metalloprotease-disintegrin ADAM8 is essential for the development of experimental asthma. *Am. J. Respir. Crit. Care Med.* **181**, 1318–1328.
- O'Shea, J.J., and Paul, W.E. (2010). Mechanisms underlying lineage commitment and plasticity of helper CD4+ T cells. *Science* **327**, 1098–1102.
- Ohoka, Y., Yokota, A., Takeuchi, H., Maeda, N., and Iwata, M. (2011). Retinoic acid-induced CCR9 expression requires transient TCR stimulation and cooperativity between NFATc2 and the retinoic acid receptor/retinoid X receptor complex. *Journal of Immunology* **186**, 733–744.
- Pahl, H.L. (1999). Activators and target genes of Rel/NF-kappaB transcription factors. *Oncogene* **18**, 6853–6866.
- Pedersen, M.B., Skov, L., Menné, T., Johansen, J.D., and Olsen, J. (2007). Gene expression time course in the human skin during elicitation of allergic contact dermatitis. *J. Invest. Dermatol.* **127**, 2585–2595.
- Perumal, N.B., and Kaplan, M.H. (2011). Regulating IL9 transcription in T helper cells. *Trends Immunol.* **32**, 146–150.
- Phan, A.T., Goldrath, A.W., and Glass, C.K. (2017). Metabolic and Epigenetic Coordination of T Cell and Macrophage Immunity. *Immunity* **46**, 714–729.
- Pino-Lagos, K., Guo, Y., Brown, C., Alexander, M.P., Elgueta, R., Bennett, K.A., De Vries, V., Nowak, E., Blomhoff, R., Sockanathan, S., et al. (2011). A retinoic acid-dependent checkpoint in the development of CD4+ T cell-mediated immunity. *J. Exp. Med.* **208**, 1767–1775.
- Rampal, R., Awasthi, A., and Ahuja, V. (2016). Retinoic acid-primed human dendritic cells inhibit Th9 cells and induce Th1/Th17 cell differentiation. *J. Leukoc. Biol.* **100**, 111–120.
- Raverdeau, M., and Mills, K.H. (2014). Modulation of T cell and innate immune responses by retinoic Acid. *Journal of Immunol.* **192**, 2953–2958.
- Reis, B.S., Rogoz, A., Costa-Pinto, F.A., Taniuchi, I., and Mucida, D. (2013). Mutual expression of the transcription factors Runx3 and ThPOK regulates intestinal CD4+ T cell immunity. *Nat. Immunol.* **14**, 271–280.
- Richard, A.C., Tan, C., Hawley, E.T., Gomez-Rodriguez, J., Goswami, R., Yang, X.P., Cruz, A.C., Penumetcha, P., Hayes, E.T., Pelletier, M., et al. (2015). The TNF-family ligand TL1A and its receptor DR3 promote T cell-mediated allergic immunopathology by enhancing differentiation and pathogenicity of IL-9-producing T cells. *Journal of Immunol.* **194**, 3567–3582.
- Schuster, G.U., Kenyon, N.J., and Stephensen, C.B. (2008). Vitamin A deficiency decreases and high dietary vitamin A increases disease severity in the mouse model of asthma. *J. Immunol.* **180**, 1834–1842.
- Sehra, S., Yao, W., Nguyen, E.T., Glosson-Byers, N.L., Akhtar, N., Zhou, B., and Kaplan, M.H. (2015). TH9 cells are required for tissue mast cell accumulation during allergic inflammation. *J. Allergy Clin. Immunol.* **136**, 433–440 e431.
- Shih, H.Y., Sciumè, G., Mikami, Y., Guo, L., Sun, H.W., Brooks, S.R., Urban, J.F., Jr., Davis, F.P., Kanno, Y., and O'Shea, J.J. (2016). Developmental Acquisition of Regulomes Underlies Innate Lymphoid Cell Functionality. *Cell* **165**, 1120–1133.
- Stephensen, C.B., Rasooly, R., Jiang, X., Ceddia, M.A., Weaver, C.T., Chandraratna, R.A.S., and Bucy, R.P. (2002). Vitamin A enhances in vitro Th2 development via retinoid X receptor pathway. *J. Immunol.* **168**, 4495–4503.
- Su, P., Chen, S., Zheng, Y.H., Zhou, H.Y., Yan, C.H., Yu, F., Zhang, Y.G., He, L., Zhang, Y., Wang, Y., et al. (2016). Novel Function of Extracellular Matrix Protein 1 in Suppressing Th17 Cell Development in Experimental Autoimmune Encephalomyelitis. *Journal of Immunol.* **197**, 1054–1064.
- Subramanian, A., Tamayo, P., Mootha, V.K., Mukherjee, S., Ebert, B.L., Gillette, M.A., Paulovich, A., Pomeroy, S.L., Golub, T.R., Lander, E.S., and Mesirov, J.P. (2005). Gene set enrichment analysis: a knowledge-based approach for interpreting genome-wide expression profiles. *Proc. Natl. Acad. Sci. USA* **102**, 15545–15550.
- Takahashi, H., Kanno, T., Nakayamada, S., Hirahara, K., Sciumè, G., Muljo, S.A., Kuchen, S., Casellas, R., Wei, L., Kanno, Y., and O'Shea, J.J. (2012). TGF-β and retinoic acid induce the microRNA miR-10a, which targets Bcl-6 and constrains the plasticity of helper T cells. *Nat. Immunol.* **13**, 587–595.
- Tripathi, S., Pohl, M.O., Zhou, Y., Rodriguez-Frandsen, A., Wang, G., Stein, D.A., Moulton, H.M., DeJesus, P., Che, J., Mulder, L.C., et al. (2015). Meta- and Orthogonal Integration of Influenza "OMICs" Data Defines a Role for UBR4 in Virus Budding. *Cell Host Microbe* **18**, 723–735.
- Troy, N.M., Hollams, E.M., Holt, P.G., and Bosco, A. (2016). Differential gene network analysis for the identification of asthma-associated therapeutic targets in allergen-specific T-helper memory responses. *BMC Med. Genomics* **9**, 9.
- Wang, H., Yang, H., Shivalila, C.S., Dawlaty, M.M., Cheng, A.W., Zhang, F., and Jaenisch, R. (2013). One-step generation of mice carrying mutations in multiple genes by CRISPR/Cas-mediated genome engineering. *Cell* **153**, 910–918.
- Wei, G., Abraham, B.J., Yagi, R., Jothi, R., Cui, K., Sharma, S., Narlikar, L., Northrup, D.L., Tang, Q., Paul, W.E., et al. (2011). Genome-wide analyses of transcription factor GATA3-mediated gene regulation in distinct T cell types. *Immunity* **35**, 299–311.
- Wilhelm, C., Hirota, K., Stieglitz, B., Van Snick, J., Tolaini, M., Lahl, K., Sparwasser, T., Helmby, H., and Stockinger, B. (2011). An IL-9 fate reporter demonstrates the induction of an innate IL-9 response in lung inflammation. *Nat. Immunol.* **12**, 1071–1077.
- Xiao, S., Jin, H., Korn, T., Liu, S.M., Oukka, M., Lim, B., and Kuchroo, V.K. (2008). Retinoic acid increases Foxp3+ regulatory T cells and inhibits development of Th17 cells by enhancing TGF-beta-driven Smad3 signaling and inhibiting IL-6 and IL-23 receptor expression. *Journal of Immunol.* **181**, 2277–2284.
- Xiao, X., Fan, Y., Li, J., Zhang, X., Lou, X., Dou, Y., Shi, X., Lan, P., Xiao, Y., Minze, L., and Li, X.C. (2018). Guidance of super-enhancers in regulation of IL-9 induction and airway inflammation. *J. Exp. Med.* **215**, 559–574.

STAR★METHODS**KEY RESOURCES TABLE**

REAGENT or RESOURCE	SOURCE	IDENTIFIER
Antibodies		
anti-GFP antibody	Biolegend	338008; RRID: AB_2563288
anti-CXCR3 antibody	Biolegend	126506; RRID: AB_1027650
anti-CCR4 antibody	Biolegend	131212; RRID: AB_2074507
Anti-CCR6 Antibody	BD Biosciences	564736; RRID: AB_2738926
anti-CD3 antibody (mouse)	BioXCell	BE0001-1; RRID: AB_1107634
anti-CD28 antibody (mouse)	BioXCell	BE0015-1; RRID: AB_1107624
anti-CD25 antibody	eBioscience	12-0251-82; RRID: AB_465607
anti-IFN- γ antibody (mouse)	BioXCell	BE0055; RRID: AB_1107694
anti-IL-4 antibody (mouse)	BioXCell	BE0045; RRID: AB_1107707
anti-CD4 antibody	eBioscience	45-0042-80; RRID: AB_906231
anti-CD44 antibody	eBioscience	56-0441-82; RRID: AB_494011
anti-CD44 antibody	eBioscience	11-0441-82; RRID: AB_465045
anti-CD45.1 antibody	eBioscience	11-0453-82; RRID: AB_465058
anti-CD45.2 antibody	eBioscience	47-0451-82; RRID: AB_1548781
anti-CD45.2 antibody	Biolegend	109830; RRID: AB_1186098
anti-CD62L antibody	eBioscience	25-0621-82; RRID: AB_469633
anti-TCR β antibody	Biolegend	109212; RRID: AB_313435
anti-Foxp3 antibody (mouse)	eBioscience	48-5773-82; RRID: AB_1518812
anti-Thy1.2 biotinylated antibody	Biolegend	140314; RRID: AB_10643274
anti-IL-9 antibody (mouse)	Biolegend	514106; RRID: AB_2562528
anti-IL-9 antibody (mouse)	Biolegend	514104; RRID: AB_2562527
anti-IL-13 antibody	eBioscience	25-7133-82; RRID: AB_2573530
anti-IL-13 antibody	eBioscience	12-7133-82; RRID: AB_763559
anti-IL-13 antibody	eBioscience	50-7133-82; RRID: AB_2574279
anti-IL-2 antibody	eBioscience	11-7021-82; RRID: AB_465382
anti-IL-17A antibody	eBioscience	11-7177-81; RRID: AB_763581
anti-IFN gamma antibody	eBioscience	12-7311-82; RRID: AB_466193
anti-CD45RO antibody (human)	Beckman Coulter	IM2712U; RRID: AB_10639537
anti-CD3 antibody (human)	BD Biosciences	557917; RRID: AB_396938
anti-IL-9 antibody (human)	Biolegend	507605; RRID: AB_315487
anti-IL-9 antibody (human)	BD Biosciences	561461; RRID: AB_10712760
anti-Foxp3 antibody (human)	eBioscience	48-4777-42; RRID: AB_1548676
anti-CD3 antibody (human)	eBioscience	14-0037-82; RRID: AB_467057
anti-CD28 antibody (human)	BD Biosciences	556620; RRID: AB_396492
anti-IFN- γ antibody (human)	BD Biosciences	564039; RRID: AB_2738557
anti-TCR β antibody	eBioscience	45-5961-82; RRID: AB_925763
anti-CD8 antibody	eBioscience	45-0081-80; RRID: AB_906236
anti-NK1.1 antibody	eBioscience	45-5941-82; RRID: AB_914361
anti-GR1 antibody	eBioscience	45-5931-80; RRID: AB_906247
anti-CD11b antibody	eBioscience	45-0112-82; RRID: AB_953558
anti-CD11c antibody	eBioscience	45-0114-82; RRID: AB_925727
anti-CD19 antibody	eBioscience	45-0193-82; RRID: AB_1106999
anti-TCR β antibody	eBioscience	47-5961-80; RRID: AB_1272209
anti-Thy1.2	eBioscience	48-0902-80; RRID: AB_1272237

(Continued on next page)

Continued

REAGENT or RESOURCE	SOURCE	IDENTIFIER
anti-CD4	BD Biosciences	560783; RRID: AB_1937327
anti-H3K27Ac	Abcam	ab4729; RRID: AB_2118291
anti-H3K4m1	Abcam	ab8895; RRID: AB_306847
anti-H3K4m3	Abcam	ab8580; RRID: AB_306649
Anti-RAR alpha	Diagenode	c15310155
anti-NRIP1	Abcam	ab42126; RRID: AB_777722
anti-STAT5A	R&D	PA-ST5A; RRID: AB_2196765
anti-STAT5B	R&D	AF1584; RRID: AB_2197076
anti-STAT6	Abcam	ab32520; RRID: AB_778113
anti-CTCF	Millipore	07-729; RRID: AB_441965
Biological Samples		
Healthy adult peripheral blood mononuclear cells	National Institutes of Health Blood Bank, this paper	N/A
Chemicals, Peptides, and Recombinant Proteins		
Recombinant Mouse IL-4	R&D	404-ML-050
Recombinant Mouse IL-12	R&D	419-ML-050
Recombinant Mouse IL-6	R&D	406-ML-050
Recombinant Human IL-2	NIH/NCI BRB Preclinical Repository	Ro 23-6019
Recombinant Human TGF-beta	R&D	240-B-010
Recombinant Human IL-4	Peprotech	200-04
Recombinant Human IL-1 beta	Peprotech	200-01B
Retinoic acid	Sigma	R2625
DMSO	Sigma	D2650
Ovalbumin peptide	Sigma	S7951
Ovalbumin	Sigma	A5503
BMS753	Tocris	3505/10
ER50891	Tocris	3823/10
Brefeldin A	BD Biosciences	555029
Phorbol 12-myristate 13-acetate (PMA)	Sigma	P1585
Ionomycin	Sigma	I3909
LIVE/DEAD Fixable Aqua Dead Cell Stain	Thermofisher	L34957
LIVE/DEAD Fixable Near-IR Dead Cell Stain	Thermofisher	L10119
Papain	Calbiochem (Millipore)	5125
Lipofectamine 2000	Thermofisher	11668019
BglII	NEB	R0144
T4 DNA ligase	NEB	M0202
Methacholine	MP Biomedicals	0219023105
Critical Commercial Assays		
NEBNext Poly(A) mRNA Magnetic Isolation kit	NEB	E7490
NEBNext Ultra II Directional RNA Library Prep kit	NEB	E7760
NEBNext Multiplex oligos for Illumina	NEB	E7335
Nextera DNA library preparation kit	Illumina	FC-121-1030
Ovation Ultralow Library System v2	Nugen	0344
Luc-Pair Duo-Luciferase Assay Kit	Genecopoeia	LPFR-P030
CD4+ T cell isolation kit, mouse	Miltenyi	130-104-454
Naive CD4+ T Cell Isolation Kit II, human	Miltenyi	130-094-131

(Continued on next page)

Continued

REAGENT or RESOURCE	SOURCE	IDENTIFIER
Deposited Data		
Raw and analyzed data	This paper	GEO: GSE123501
ENSEMBL release 82 GRCh38		http://www.ensembl.org//useast.ensembl.org/index.html?redirectsrc=/www.ensembl.org%2Findex.html
ChIP-seq samples for STAT5B and STAT6	Liao et al., 2014	http://www.ncbi.nlm.nih.gov/geo ; GEO: GSE41317
ATAC-seq samples for various cell types	Shih et al., 2016	http://www.ncbi.nlm.nih.gov/geo ; GEO: GSE77695
Microarray samples for human CD4 T cells cultured with housedust mite vs. vehicle control	Troy et al., 2016	http://www.ncbi.nlm.nih.gov/geo ; GEO: GSE73482
Microarray samples for nickel exposed human skin	Pedersen et al., 2007	http://www.ncbi.nlm.nih.gov/geo ; GEO: GDS2935
Microarray samples for Th subsets	Jabeen et al., 2013	http://www.ncbi.nlm.nih.gov/geo ; GEO: GSE44937
RNA-seq samples of IL-2 treated WT and STAT5-deficient CD4 ⁺ T cells		http://www.ncbi.nlm.nih.gov/geo ; GEO: GSE77656
Microarray samples of WT and STAT6-deficient T cells cultured for 7 days in Th2 conditions	Wei et al., 2011	http://www.ncbi.nlm.nih.gov/geo ; GEO: GSE22081
RNA-seq samples of WT and GATA3-deficient CD4 ⁺ T cells cultured under Th2 conditions	Wei et al., 2011	http://www.ncbi.nlm.nih.gov/geo ; GEO: GSE20898
Microarray samples of WT and SMAD3-deficient T cells stimulated with TGF beta		http://www.ncbi.nlm.nih.gov/geo ; GEO: GSE19601
Microarray samples of CD4 ⁺ T cells gene-transduced with AML1 (Runx1) or empty vector		http://www.ncbi.nlm.nih.gov/geo ; GEO: GSE6939
RNA-seq samples of WT, Irf4 ^{-/-} and Batf ^{-/-} mice in CD4 ⁺ T cells	Li et al., 2013	http://www.ncbi.nlm.nih.gov/geo ; GEO: GSE39756
ChIP-seq and RNA-seq samples of CD4 ⁺ T cells deficient in Irf4, Fosl2, Batf, Hif1a, Ikzf3, Mac, or Rorc		http://www.ncbi.nlm.nih.gov/geo ; GEO: GSE40918
Microarray samples of WT and ATF3 deficient bone marrow derived macrophages		http://www.ncbi.nlm.nih.gov/geo ; GEO: GSE61055
Microarray samples of WT and VDR deficient macrophages		http://www.ncbi.nlm.nih.gov/geo ; GEO: GSE2421
Microarray samples of WT and Foxp-deficient Tfh cells	Wang et al., 2013	http://www.ncbi.nlm.nih.gov/geo ; GEO: GSE50725
Microarray samples of WT and Nfat1-deficient CD8 ⁺ T cells		http://www.ncbi.nlm.nih.gov/geo ; GEO: GSE64409
RNA-seq samples of WT and JunB deficient Th17 cells		http://www.ncbi.nlm.nih.gov/geo ; GEO: GSE98413
Experimental Models: Cell Lines		
Human: HEK293T cells	ATCC	CRL-3216
Experimental Models: Organisms/Strains		
C57BL/6J	The Jackson Laboratory	#000664
B6.SJL-PtprcaPep3b/BoyJ (CD45.1+)	The Jackson Laboratory	#002014
B6.129S6-Rag2 ^{tm1Fwa} Tg(TcraTcrb)425Cbn	Taconic	#11490-M
B6.Cg-Foxp3 ^{sf/J}	The Jackson Laboratory	#004088
Rara ^{tm3Ipc}	Hall et al., 2011a	MGI ID: 238606
Tg(Cd4-cre)1Cwi/BfluJ	The Jackson Laboratory	#017336
II9.E1 ^{-/-}	This paper	N/A
II9.E2 ^{-/-}	This paper	N/A
II9 ^{tm2.1Flv} (INFER)	Licona-Limón et al., 2013	MGI ID: 5568755
B6.Cg-Tg(II9-cre) #Stck/J	The Jackson Laboratory	#024474
Oligonucleotides		
Primers for ChIP-qPCR of II9 locus, see table S2	IDT	Table S2
Primers for 3C of II9 locus, see table S2	IDT	Table S2
Probe for 3C of II9 locus, see table S2	IDT	Table S2
Proximal sgRNA for E1 deletion: CCACCTGCTATGAAATGGCATGA	This paper	See sequence

(Continued on next page)

Continued

REAGENT or RESOURCE	SOURCE	IDENTIFIER
Distal sgRNA for E1 deletion: CGCAACCTTGTAGCAACTTGAGG	This paper	See sequence
Proximal sgRNA for E2/E3 deletion: CCTGTCTCGGCCAGGAGCTCT	This paper	See sequence
Distal sgRNA for E2/E3 deletion: TCCTATCCAGACATTGAGGCTGG	This paper	See sequence
Recombinant DNA		
Bacterial Artificial Chromosome: Clone CH29-537K21 (Chr13: 56,468,749 - 56,674,596)	Children's Hospital Oakland Research Institute	CH29-537K21
pGL4.23	Promega	9PIE841
pRL-TK	Promega	E2231
Luciferase constructs for Figure S5, see Table S3	GeneCopoeia	Table S3
Software and Algorithms		
STAR Aligner v2.4.2a		https://github.com/alexdobin/STAR
BEDTOOLS v2.15		https://bedtools.readthedocs.io/en/latest/index.html
wigToBigWig		https://genome.ucsc.edu/goldenpath/help/bigWig.html
The Integrative Genomics Viewer (IGV)		http://software.broadinstitute.org/software/igv/
kallisto v0.42.4		https://pachterlab.github.io/kallisto/
pheatmap R package	Raivo Kolde	https://cran.r-project.org/web/packages/pheatmap/index.html
GOstats R package		https://www.bioconductor.org/packages/release/bioc/html/GOstats.html
Bowtie2-2.1.0		http://bowtie-bio.sourceforge.net/index.shtml
Bowtie 0.12.8		http://bowtie-bio.sourceforge.net/index.shtml
HOMER v4.8		http://homer.ucsd.edu/homer/
MACS v 1.4.3		http://lilab.dfci.harvard.edu/MACS/index.html
BEDTOOLS v2.24		https://bedtools.readthedocs.io/en/latest/
bcl2fastq 2.17.1	Illumina, Inc.	https://support.illumina.com/sequencing/sequencing_software/bcl2fastq-conversion-software.html
Partek Genomics Suite 6.6	Partek, Inc.	http://www.partek.com/partek-genomics-suite/
Morpheus	Broad Institute	https://software.broadinstitute.org/morpheus
R 3.0.1	The R project	https://www.r-project.org
Metascape	OMICtools	http://metascape.org
GSEA software	Broad Institute	http://software.broadinstitute.org/gsea/index.jsp
bioDBnet	National Cancer Institute	https://biodbnet-abcc.ncifcrf.gov
Crossmap		http://crossmap.sourceforge.net
FlowJo	FlowJo, LLC	https://www.flowjo.com
Prism	GraphPad	https://www.graphpad.com/scientific-software/prism/
Rstudio	Rstudio team	https://www.rstudio.com/
TopHat 2.0.8	Johns Hopkins University CCB	https://ccb.jhu.edu/software/tophat/index.shtml
Other		
N/A	N/A	N/A

CONTACT FOR REAGENT AND RESOURCE SHARING

Further information and requests for resources and reagents should be directed to and will be fulfilled by the corresponding author, Daniella M. Schwartz (daniella.schwartz@nih.gov).

EXPERIMENTAL MODEL AND SUBJECT DETAILS

All human peripheral blood samples were obtained from buffy coats from normal donors; all studies were approved by the Institutional Review Board of the National Institutes of Health. All animal experiments were performed in the AAALAC-accredited animal housing facilities at NIH. All animal experiments were conducted in accordance with NIH guidelines for the use and care of live animals and were approved by the Institutional Animal Care and Use Committee of the National Institute of Arthritis and Musculoskeletal and Skin Diseases (NIAMS). Mice were bred and maintained at the National Institutes of Health specific pathogen free animal facility, in conventional open cages. Food and water were continuously available, mice were maintained on a 12-hour light/dark cycle, and mice were checked periodically to ensure normal health, and checked daily if adverse effects were anticipated.

All mice were on a C57Bl/6 background. *Foxp3^{Sf}*, eYFP IL-9 fate reporter, and B6 CD45.1 mice were purchased from the Jackson Laboratory. *Rag2^{-/-}* OT-II mice were purchased from Taconic Biosciences. *Rara^{-/-}* mice were graciously provided by Yasmine Belkaid, INFER mice were graciously provided by Richard Flavell. Enhancer knockout mice were generated by the NHLBI Crispr Core Facility (see below). Mice were genotyped by standard PCR protocols.

3-6 replicates were used for all *in vitro* experiments except for sequencing experiments (RNA-seq, ChIP-seq, ATAC-seq), where 2-3 replicates were used. For all papain experiments where Th9 cells were isolated from lung, 2-4 separate experiments were performed, with 3-5 subjects per experimental group (18-20 subjects per experiment). For flexivent experiments, 2-3 replicates with 1-3 subjects per experimental group (9-10 subjects per experiment) were performed. For Th9 transfer experiments, two separate experiments with 1-3 subjects per experimental group (6-10 subjects per experiment) were performed.

The majority of experiments were performed on 8-14-week-old mice, with the exception of the flexivent experiments, which were performed on 12-18-week-old mice. Experiments on *Foxp3^{Sf}* mice and *Foxp3^{WT}* littermate controls were done in male mice because the *Foxp3^{Sf}* allele is X-linked and the experiments could not be done in female mice. Th9 transfer experiments were all done in male mice because *Foxp3^{Sf}* donor Th9 cells were obtained from male mice and could not be transferred to female recipients due to risk of rejection. All remaining experiments were done in both male and female mice and were age and sex-matched within experiments.

METHOD DETAILS

Generation of Enhancer Knockout Mice

The *Il9.E1^{-/-}* and *Il9.E2E3^{-/-}* mice were generated using the CRISPR/Cas9 method as reported previously (Wang et al., 2013). Briefly, for each line, an upstream sgRNA (AGAGCTCCTGGGGCCGAGAC) and a downstream sgRNA (TCCTATCCAGACATTGAGGC) were made using T7 promoter-driven *in vitro* transcription. These two sgRNAs (5 ng/ul each) were co-microinjected with Cas9 mRNA (10 ng/ul, purchased from Trilink Biotechnologies) into the cytoplasm of fertilized eggs collected from C57BL/6N mice (Charles River). The injected zygotes were cultured overnight in M16 medium at 37°C in 5% CO₂. The next morning, embryos that had reached the 2-cell stage of development were implanted into the oviducts of pseudopregnant foster mothers (Swiss Webster, Taconic Farm). The mice born to the foster mothers were genotyped using PCR, and then confirmed by DNA sequencing. Founder mice with the desired mutations, resulting in deletion of either entire enhancer E1 (3kb deletion) or the contiguous enhancer E2-E3 region (8kb deletion), were bred with C57BL/6N mice for propagating the line, as well as for eliminating possible mosaicism and diluting out off-target effects, if any. Germline transmission of the E1 deletion (*Il9.E1^{-/-}* mice) and the E2-E3 region (*Il9.E2E3^{-/-}*) mice was confirmed by DNA sequencing after 4 generations of breeding.

Media

All cell cultures were performed in RPMI medium with 10% (vol/vol) FCS (Invitrogen), 2 mM glutamine (Invitrogen), 100 IU/mL penicillin (Invitrogen), 0.1 mg/mL streptomycin (Invitrogen), 20 mM HEPES buffer (pH 7.2–7.5) (Invitrogen), and 2 mM β-mercaptoethanol (Sigma-Aldrich).

Reagents

RA was purchased from Sigma (cat#R2625) and reconstituted in DMSO at a stock concentration of 100mM (*in vitro* experiments) or 40mg/mL (*in vivo* experiments). BMS753 (Tocris cat#3505) and ER50891 Tocris (cat#3823) were reconstituted in DMSO to stock concentrations of 100mM. Aliquots of RA and agonists/antagonists were serially diluted in PBS immediately prior to *in vitro* treatment of cells. Stocks were replaced every 3-6 months.

Cell Culture

Naïve CD4⁺/CD25⁻/CD44^{lo}/CD62L^{hi} mouse T cells were isolated by cell sorting from spleen and lymph nodes to >95% purity using a FACSAria III Cell Sorter, after magnetic enrichment (StemCell Technologies or Miltenyi Biotec). T cells were plated at a density of 0.5x10⁶/mL and activated with 10μg/mL plate bound anti-CD3/ anti-CD28 for 72h in the presence of polarizing cytokines and

antibodies to promote the differentiation of Th0 (none), Th1 (10ng/mL IL-12, 10 µg/mL anti-IL-4), Th2 (20 ng/mL IL-4, 10 µg/mL anti-IFN-gamma, Th9 (20ng/mL IL-4, 10 µg/mL anti-IFN-gamma, 2.5 ng/mL TGF-beta, 100 units/mL hIL-2), Th17 (10ng/mL IL-6, 10µg/mL anti- IFN-gamma, 10µg/mL anti-IL-4, 2.5ng/mL TGF-beta), iTreg (10ng/mL TGF-beta, 100 units/mL hIL-2).

For experiments examining the effects of RA on established Th9 cells, naïve T cells were purified and cultured to promote Th9 differentiation, adding either DMSO or RA (1 µM) on d0 of culture. After 72 hours, cells were harvested, washed, and resuspended in Th9-promoting cytokines and antibodies. Cells were split to two aliquots of 0.5×10^6 cells/mL on 10 µg/mL plate bound anti-CD3/anti-CD28. One aliquot was maintained under the same culture conditions (control → control or RA → RA) and one aliquot was switched to different culture conditions (control → RA or RA → control). Cytokine production was assessed by intracellular staining on d6 of culture.

For transfer experiments, antigen presenting cells (APCs) from C57Bl/6 mice were depleted of T-cells by magnetic separation (Miltenyi) using biotinylated anti-Thy1.2 (53-2.1, Biolegend). T-cell depleted APCs (> 95% purity) were resuspended to a density of 2 million/mL in complete RPMI and irradiated at 3000 Gray. *Rag2^{-/-}* OT-II Foxp3^{Sf} CD45.2⁺ CD4⁺ T cells were isolated in vitro using magnetic enrichment and cultured in complete IMDM under the following conditions: 1:5 CD4⁺ T cells:T-cell depleted irradiated APCs, 10ng/mL IL-4, 2ng/mL human TGF-β, 0.5µg/mL soluble anti-CD28, 10µg/mL anti-IFN-γ, 1µM ovalbumin peptide (S7951, Sigma).

For human T cell cultures, peripheral blood mononuclear cells (PBMCs) from de-identified healthy donors were obtained from the NIH Blood Bank, isolated using Ficoll, and frozen in liquid nitrogen for up to 6 months. PBMCs were thawed, and CD45RA⁺ CD45RO⁻ CD4⁺ T cells were isolated using magnetic columns (Miltenyi) to >90% purity. T cells were plated at a density of 1×10^6 cells/mL and activated with 1 µg/mL plate bound anti-CD3 (ebioscience clone OKT3) and 0.5 µg/mL soluble anti-CD28 (BD clone L293) for 5 days in the presence of polarizing cytokines and antibodies to promote Th9 differentiation (30 ng/mL IL-4, 5 µg/mL anti-IFN-gamma (BD clone B27), 5 ng/mL TGF-beta, 10 ng/mL IL1β, 10 units/ml IL-2).

Anti-CD3, anti-CD28, anti-IFN-gamma and anti-IL-4 were purchased from BioXcell, human IL-2 was purchased from the NIH/NCI BRB Preclinical Repository, and all other mouse antibodies and cytokines were purchased from R&D Systems. Human cytokines were purchased from Peprotech, and antibodies were purchased from BD unless otherwise specified. Where specified, RA (0.1nM-1µM as specified), DMSO (vehicle control), BMS753 (RARα agonist), or ER50891 (RARα antagonist) were added on d0 of culture. Concentrations of RARα selective agonists and antagonists were chosen based on IC50 data provided by the manufacturer.

Flow Cytometry

For analysis of cytokine production, cells were stimulated in 96-well plates for 4-6 hours with phorbol 12-myristate 13-acetate (PMA), ionomycin (50ng/mL and 500ng/mL, respectively), treated with brefeldin A (10 µg/mL; Sigma Aldrich) Cells were stained with LIVE/DEAD Cell Stain (Invitrogen), followed by staining for cell surface markers, and then fixed and permeabilized with the Cytofix/Cytoperm kit (BD Biosciences, Cat# 554714) for intracellular staining.

Viability was assessed with LIVE/DEAD Fixable Aqua Dead Cell Stain or LIVE/DEAD Fixable Near-IR Dead Cell Stain (ThermoFisher).

For intracellular staining of *in vitro* cultured mouse cells, the following antibodies were used: anti-IL-9 PE or APC (RM9A4 and D9302C12); anti-IL-13 PE-Cy7 (eBio13A); anti-IL-17 FITC (eBio17B7, eBiosciences); anti-IFN-gamma PE (XMG1.2); anti-Foxp3 eFluor 450 (FJK-16s), anti-CD4 PerCp-Cy5.5 (RM4-5). For intracellular staining of *in vitro* cultured human cells, the following antibodies were used: anti-IL-9 PE or PerCP-Cy5.5 (MH9A4 or MH9A3, BD or Biolegend), anti-CD3 Alexa Fluor 700 (SP34-2, BD), anti-Foxp3 eFluor 450 (236A/E7, eBioscience), anti-CD45RO PE-Texas Red (UCHL1, Beckman Coulter).

Cells extracted from lung tissue were stained with LIVE/DEAD Fixable Blue Dead Cell Stain (Life Technologies), and with antibodies against the following cell surface markers for lineage negative selection: TCR-β, CD8, NK1.1, GR1, CD11b, CD11c, and CD19 (PerCp-Cy5.5, eBioscience). Cells were also stained with the following antibodies TCRβ APC-eFluor 780 (eBioscience), CD45.2 PeCy7 (BioLegend), Thy1.2 eFluor 450 (eBiosciences), CD44 AlexaFluor 700 (eBioscience), CD4 V500 (BD), IL-9 PE (BioLegend) or IL-9 APC (eBioscience), IL-13 PE or IL-13 eFluor 660 (eBioscience), IL-17 FITC (eBioscience) or IL-2 FITC (eBioscience), Foxp3 v450 (eBioscience). For Th9 transfer experiments, the following panel was used: CD45.1 FITC (eBioscience), CD45.2 APC-eFluor780 (eBioscience), TCRβ APC (Biolegend), CD4 PerCp-Cy5.5 (Biolegend), IL-9 PE (BioLegend), and Foxp3 v450 (eBioscience). For isolation and sorting of ex vivo Th9 cells and other Th subsets, antibodies against the following antigens were used on unstimulated cells: CD45.2 PeCy7 (eBioscience), TCRβ APC-eFluor 780 (Biolegend), CD44 AlexaFluor 700 (eBioscience), CD4 PerCp-Cy5.5 (Biolegend), GFP/YFP AlexaFluor 488 (Biolegend), CXCR3 PE (Biolegend), CCR4 APC (Biolegend), CCR6 Brilliant Violet 421 (BD).

Data were collected on a FACS Verse or LSR Fortessa (BD Biosciences) and analyzed using Flowjo software (Tree Star).

RNA-seq

For *in vitro* polarized cells, total RNA was prepared from approximately 500,000 cells using an Ambion mirVana miRNA isolation kit following the manufacturer's protocol (ThermoFisher AM1560). For *in vivo* IL-9 producing cells and other subsets, total RNA was prepared from approximately 2,000-10,000 cells using a Trizol-based extraction technique following the manufacturer's protocol (ThermoFisher 15596026). For all samples, mRNA was processed to generate single end mRNA-seq libraries using NEBNext Poly(A) mRNA Magnetic Isolation and Ultra II Directional RNA Library Prep kit for Illumina (NEB E7490, E7760, E7335). After recovering purified DNA, libraries were generated according to the vendor's manual for the Illumina platform. Illumina HiSeq 2500 was used for 50-cycle single-end read sequencing. Raw sequencing data were processed with bcl2fastq 2.17.1 to generate FastQ files.

ATAC-seq

ATAC-seq samples were prepared as previously described (Shih et al., 2016). Briefly, cells were harvested after 72 hours of culture, and dead cells were removed by flow cytometric sorting. Approximately 50,000 cells were isolated, washed with cold PBS, and lysed for 10 minutes in cold lysis buffer (10 mM Tris-HCl [pH 7.4], 10 mM NaCl, 3 mM MgCl₂, 0.1% IGEPAL CA-630). After pelleting the nuclei by centrifugation (500×g for 10 min), pellets were resuspended in a 40-μl transposition reaction with 2 μl Tn5 transposase (FC-121-1030; Illumina) to tag and fragmentize accessible chromatin. The reaction was incubated at 37°C, 400 rpm for 30 min; DNA was then purified using a MinElute kit (QIAGEN) and amplified with 8-12 cycles of PCR based on the amplification curve. After purification using a QIAquick PCR cleanup kit (QIAGEN) and Ampure XP beads (Beckman Coulter), samples were sequenced for 75 cycles (paired-end reads) on an Illumina HiSeq 2500.

Histone Chromatin Immunoprecipitation and ChIP-seq

ChIP-seq and ChIP-qPCR were performed using in vitro differentiated Th9 cells treated with RA 1μM or DMSO control. At least 20 million cells were used for transcription factor ChIP, and at least 1 million cells were used for histone mark ChIP. After chemical chromatin cross-linking (1% formaldehyde), cells were washed and frozen at -80°C for ≤6 months.

Sonication: Histone Chromatin Immunoprecipitation

Cells were resuspended in high SDS shearing buffer (50mM Tris-HCl, 10mM EDTA, 1% SDS, protease inhibitors) at a concentration of 10 million/mL, and DNA fragmentation was performed on a Diagenode Bioruptor at high amplitude (40 cycles, 30s on/30s off) to an average length of 200-500 bp. After sonication, lysates were diluted to 0.1% SDS for immunoprecipitation.

Transcription Factor Chromatin Immunoprecipitation and ChIP-qPCR

20 million cells were suspended in 10 mL cell lysis buffer (50mM HEPES-KOH, 140mM NaCl, 1mM EDTA, 10% Glycerol, 0.5% Triton-X-100, Roche Complete mini EDTA free tablet 10X #11836170001) for 10 minutes at 4°C, pelleted, resuspended in 5 mL protein extraction buffer (200mM NaCl, 1mM EDTA, 0.5mM EGTA, 10mM Tris pH8) for 10 minutes at room temperature. Cells were pelleted and resuspended in 0.5 mL chromatin extraction buffer (protein extraction buffer with 0.1% Na-Deoxycholate, 0.5% N-laurylsarcosine, 0.1% SDS) and sonicated using a Bioruptor sonicator (high frequency, 30s on/30s off, 40 cycles) to a major band size of 300-500bp.

Immunoprecipitation, Library Preparation, and ChIP-qPCR

After sonication, cells were immunoprecipitated with anti-H3K27Ac (ab4729; Abcam), anti-H3K4m1 (ab8895; Abcam), anti-H3K4m3 (ab8580; Abcam), anti-RAR α (c15310155; Diagenode), anti-NRIP1 (ab42126; Abcam), a 1:1 mix of anti-STAT5A(PA-ST5A; R&D Systems)/anti-STAT5B (AF1584, R&D Systems), anti-STAT6 (ab32520; Abcam), or anti-CTCF (07-729; Millipore). Aliquots of genomic DNA (input) and immunoprecipitated samples were treated with proteinase K, heated to induce de-cross linking, and purified using columns (D4014, Zymo). After recovering purified DNA, 5ng or more of DNA was used to generate libraries according to the vendor's manual for the Illumina platform (Cat#0344; NuGEN). Illumina HiSeq 2500 was used for 50-cycle single-read sequencing.

For ChIP-qPCR, quantitative PCR reactions were performed in triplicate on specific genomic regions using SYBR Green supermix (Bio-Rad). See STAR Methods Table for primer details. Data was normalized for primer efficiency by carrying out reactions on input DNA and normalizing relative to input signal. For all reactions, an inaccessible region within the *I/I9* locus (gene desert) was used as a negative control for normalization.

Cell Lines and Transfection

HEK293T cells were obtained from ATCC and maintained in DMEM supplemented with 10% FBS and antibiotics. Cells were transfected using lipofectamine 2000 (cat#11668019; ThermoFisher) per the manufacturer's protocol.

Luciferase Detection

The *I/I9* promoter was cloned either alone or in tandem with E1, E2, or E3 into pGL4.23, a luciferase reporter vector with a minimal promoter. Sequences of specific constructs are provided in the Supplementary Data. We transfected HEK293T cells with each construct, and co-transfected cells with constitutively active Stat5A. Cells were also co-transfected with pRL-TK (Renilla luciferase vector) for background normalization. After 48 hours, cells were lysed, and luciferase activity was detected using the Genecopoeia Luc-Pair Duo-Luciferase Assay Kit (Cat# LPFR-P030).

Chromatin Conformational Capture (3C)

3C was performed using in vitro differentiated Th0 cells, Th9 cells treated with RA 1μM, or Th9 cells treated with DMSO control. At least 10 million cells were used for each condition. After chemical chromatin cross-linking (1% formaldehyde), cells were washed and lysed (10mM Tris pH8, 10mM NaCl, 0.2% NP-40). Crosslinked DNA digested overnight at 37°C with 200 units of restriction enzyme (BglII, R0144L), then digested for another 24 hours with 200 additional units. Digestion efficiency was determined to be >95%. Restriction enzyme was heat-inactivated at 68°C for 10 minutes, and fragments were religated (T4 ligase, 100 weiss units) at 16°C overnight, after which an additional 100 units of T4 ligase was added for 4 hours. Crosslinking was reversed, after which

DNA was isolated and purified for analysis using RT-qPCR. A bacterial artificial chromosome (BAC) containing the *Ilo* locus and surrounding gene loci was used for quantification. Primers and probes for the *Fbxl21* locus, which is adjacent to *Ilo* and which was not affected by RA, were used for normalization. Primer and probe information are provided in STAR Methods Table.

Papain Induced Asthma

For papain-induced lung inflammation, mice were anaesthetized with isoflurane and exposed intranasally to 25 µg papain (Calbiochem) in 30 µL PBS on day 0, 3, 6 and 14. 12–16 hours after the last challenge, lung-isolated cell analyses, and/or measurements of airway reactivity were performed.

Lung tissues were fixed in 4% neutral buffered formaldehyde, embedded in paraffin, sectioned, and stained with hematoxilin and eosin (H&E) or periodic acid-Schiff (PAS) stain. Cells were isolated from lungs by incubating lung fragments with 100U collagenase for 1 hour and 10 min. Lung cells were stained for surface antigens and intracellular cytokines after stimulation with PMA/ionomycin for 4–5 hours, as detailed above.

Th9 Transfer Experiment

For Th9 transfer experiments, *Rag2*^{−/−} OT-II Foxp3^{Sf} (ovalbumin specific) Th9 cells were cultured in vitro in the presence of either vehicle control or RA 1µM as detailed above. After 72 hours, Th9 cells were harvested and washed three times with PBS, and then 0.9 million Th9 cells were injected into the tail veins of B6 CD45.1 mice. On day 1 after Th9 transfer, mice were anaesthetized by i.p. administration of ketamine/xylazine mixture (1 mL ketamine [100 mg/mL], 0.5 mL xylazine [20 mg/mL], and 8.5 mL PBS) and challenged intratracheally with 100µg of ovalbumin (Sigma-Aldrich A5503-50G). On day 2, were anaesthetized with isoflurane and challenged intranasally with 100µg of ovalbumin; 12–20 hours after the last challenge, lung-isolated cell analyses were performed as detailed above.

Measurement of Allergic Airway Reactivity

For RA treatment experiments, mice were anaesthetized with isoflurane and exposed intranasally to 25 µg papain as detailed above. For experiments in WT versus RAR α -/- mice, 12.5µg papain was used but the same volume/schedule was maintained, due to high amounts of mucus plugging noted in histology slides with full-dose (25µg) papain, which limits the sensitivity of airway reactivity measurement. Bronchial reactivity was determined 12–18h after the last challenge of papain. Mice were anaesthetized by i.p. administration of ketamine/xylazine mixture (1 mL ketamine [100 mg/mL], 0.5 mL xylazine [20 mg/mL], and 8.5 mL PBS). A 19-gauge blunt-end needle was inserted into the trachea, and the animals then were ventilated mechanically. Baseline measurements were recorded after the aerosol administration of saline, followed by doubling doses of methacholine (6.25–100 mg/mL) using flexiVent (Scireq Scientific Respiratory Equipment).

QUANTIFICATION AND STATISTICAL ANALYSIS

RNA-seq Analysis

Reads of 50 bases were mapped to the mouse transcriptome and genome mm9 using TopHat 2.0.8 with Bowtie2-2.1.0. Gene expression values (RPKM: Reads Per Kilobase exon per Million mapped reads) were calculated with Partek Genomics Suite 6.6. 2–3 replicate RNA-seq experiments were performed for each condition.

Datasets were normalized based on RPKM and purged of micro-RNAs, sno-RNAs and sca-RNAs. To minimize fold-change artifact from low abundance transcripts, a small offset was added to all RPKM values (equal to the averaged second quartiles of each dataset). When multiple transcripts were detected for a single gene, only the most abundant (highest average RPKM across all replicates) was analyzed. Transcripts with RPKM < 1 were excluded. Heatmaps were created using Morpheus (Broad Institute). Other downstream analyses and figures were created with R 3.0.1 and custom R programs, unless otherwise specified.

Cell-Specific and Shared RA-Regulated Modules

Individual lists of RA-regulated genes were generated separately for each subset (Th0, Th1, Th2, Th9, Th17, and iTreg). Differential gene expression was determined by ANOVA using FDR <0.05 and 2-fold change relative to vehicle-treated controls (Partek Genomics Suite). The six gene lists were combined, and duplicates were removed, to generate a master set of 1025 RA-regulated targets genes. K-means clustering ($k=15$) was performed based on fold-change in gene expression (RA versus vehicle control). K-means clusters (Table S1) were defined as regulated in multiple subsets if $\geq 50\%$ of the genes were RA-regulated (FDR<0.05) in ≥ 3 subsets and regulated in a subset-specific fashion if $\geq 50\%$ of the genes were RA-regulated in ≤ 2 subsets.

Evaluation of Functional Enrichment

All we identified Kegg Pathway and Gene Ontology terms enriched in sets of differentially expressed genes using metascape (<http://metascape.org>). Complete lists of enriched pathways are included in Table S1.

Gene Sensitivity Enrichment Analysis

GSEA analysis was performed as described (Subramanian et al., 2005). Enrichment score curves and member ranks were generated by the GSEA software (Broad Institute). RNA-seq datasets were used in conjunction with the following user-generated Gene

Sets (1) Th9-high genes based on the overlap of *in vitro* and *in vivo* data. For *in vitro* data, Th9-high genes were defined as FDR<0.05 and average gene expression \geq 1.5 fold higher in Th9 cells using a 1-way ANOVA of Th9 cells versus (Th1 or Th2 or Th17 or iTreg cells). For INFER (GFP IL-9 reporter) mice, Th9-high genes were defined as FDR<0.05 and average gene expression \geq 1.5 fold higher in GFP $^+$ cells compared with GFP $^-$ cells. For eYFP IL-9 fate reporter mice, Th9-high genes were defined as FDR<0.05 and average gene expression \geq 1.5 fold higher in *Il9*-expressing subsets (eYFP $^+$ or Th2) cells compared non-*Il9*-expressing (Th1 and Th17) subsets. Genes that were identified as Th9-high in the *in vitro* dataset and in at least one *in vivo* dataset were included in the Th9-high gene cassette (2) Th9 high genes based on a more stringent analysis of *in vitro* data, defined as FDR<0.05 for Th9 versus Th1, Th2, Th17, and iTreg subsets by 1-way ANOVA; average gene expression \geq 1.5 fold higher in Th9 cells using pairwise comparisons of Th9 versus Th1, Th9 versus Th2, Th9 versus Th17, and Th9 versus iTreg subsets; rpkm>5 in Th9 cells (30 members) (3) Th9 genes as defined by a separate dataset (GSE44937). Because this dataset did not test relevant comparators (Th1, Th17 subsets), genes associated with these subsets were manually removed prior to analysis. For **Figure S7**, gene lists from Th9/iTreg-selective and common RA-regulated modules were converted to human orthologs using bioDBnet and combined to generate a list of 335 human orthologs of murine RA-induced genes and 353 human orthologs of murine RA-repressed genes.

For **Figure 2**, lists of TF-induced and TF-repressed genes were obtained by analyzing public datasets: (1) IL-2 regulated Stat5 target genes (GSE77656, 420 genes) (2) IL-4 regulated Stat6 target genes (GSE22801, 251 genes) (3) IL-4 regulated Gata3 target genes (GSE20898, 623 genes) (4) TGF- β regulated Smad3 target genes (GSE19601, 323 genes), (5) Runx1 target genes (GSE6939, 715 genes), (6) Irf4 target genes (GSE39756, 862 genes) (7) canonical NF- κ B target genes ([\(Pahl, 1999\)](#), 177 genes), (8) Fosl2 target genes (GSE40918, 95 genes), (9) Atf3 (GSE61055, 46 genes), (10) Vdr target genes in macrophages (GSE2421, 2373 genes), (11) Foxp1 (GSE50725, 60 genes), (12) Nfat target genes in CD8 T cells (GSE64409, 209 genes), (13) Batf target genes in Th17 cells (GSE40918, 156 genes), (14) Junb (GSE98413, 233 genes), (15) Rorc target genes in Th17 cells (GSE40918, 78 genes). Normalized Enrichment Scores for TF-induced and TF-repressed genes were combined to generate a consensus enrichment score. Significance was determined by combining FDR for the two GSEA analyses using Fisher's method for combining independent tests.

Selection and Analysis of Human Datasets

The Gene Expression Omnibus was searched for datasets or series examining time-course gene expression in atopic or allergic inflammation, which displayed significantly increased *IL9* expression during allergic response. Ratios of mean gene expression values at two timepoints were calculated in Partek. To determine the effect of allergen on RA-regulated genes, gene lists from Th9/iTreg-selective and common RA-regulated modules were converted to human orthologs using bioDBnet, to obtain a list of 688 human orthologs of murine RA-regulated genes. Human gene expression arrays were filtered for RA-regulated genes using RStudio: 645 RA-regulated genes were expressed in GSE73482 whereas 665 RA-regulated genes were expressed in GDS2935. Lack of expression was confirmed manually for each of the undetected genes in both datasets. Ecdf (empirical cumulative distribution function) plots were generated in RStudio.

ChIP-seq Alignment and Peak Calling

Reads of 50 bases were aligned to the mouse genome build mm9 with Bowtie 0.12.8, allowing two mismatches. Uniquely mapped and non-redundant reads were used for downstream analysis. The aligned file was converted to bam format using samtools (<http://samtools.sourceforge.net>). Peaks were called using MACS v1.4.3 using a p<1e-5 and with the input sample for background correction. In the case of H3K4me1, H3K4me3, and H3K27Ac samples, “—nomodel” setting was used. BigWig tracks were generated from Bam files and converted into bedGraph format using bedtools. These were further reformatted with the UCSC tool bedGraphToBigWig. Genome browser files are displayed with IGV.

For STAT5 and STAT6 ChIP-seq data in Th9 cells, raw data were downloaded from the Gene Expression Omnibus (GSE41317). Annotation was converted to mm9 (crossmap), files were processed as above, and tdf files were generated from bedGraph files using igvtools.

ATAC-seq Alignment and Peak Calling

ATAC-seq reads from two biological replicates were used for each sample. Redundant paired-end (PE) reads were removed using fastquniq. PE reads of 50 bases were aligned to the mouse genome build mm9 with Bowtie 0.12.8, following the guidelines presented by Buenrostro et al ([Buenrostro et al., 2013](#)). Customized python scripts were used to calculate fragment length of each pair of uniquely mapped PE reads for size distribution analysis, and to group uniquely mapped reads into bins of 0 to 175 bases and 180 to 250 bases, respectively. UCSC Genome Browser viewable and normalized BigWig files were generated with the Hypergeometric Optimization of Motif EnRichment program (HOMER) version 4.8.

Only one mapped read to each unique region of the genome that was less than 175 bp was kept and used in peak calling. Regions of open chromatin were identified by MACS (version 1.4.3) using a p-value threshold of 1×10^{-5} . Only regions called in both replicates were used in downstream analysis. Peak intensities (“tags” column) were normalized as tags per 10 million reads (RP10M) in the original library.

Analysis of ATAC-seq and ChIP-seq Peaks

Signal across all sites (i.e., all annotated genes and all accessible chromatin regions) was analyzed to eliminate potential bias by pre-selection. After calling ATAC-seq peaks with MACS, the union peaks of replicate samples were created using mergePeaks module in HOMER and divided into shared and cell-specific peaks using the same utility. For analysis of chromatin accessibility and epigenetic marks associated with Th9-high genes, peaks were annotated based on proximity to the nearest gene, and tag densities (normalized reads) were calculated using HOMER. For ATAC-seq data, fold-changes in tag density were calculated for RA-treated versus control-treated WT Th9 cells and for RAR α^{ACD4} Th9 cells. For ChIP-seq data, tag densities for immunoprecipitated samples were normalized to paired input controls; then fold-changes in normalized tag density were calculated for RA-treated versus control-treated WT Th9 cells and for RAR α^{ACD4} Th9 cells. When multiple peaks were annotated to a single gene, the peak with the highest absolute fold change (RA versus control) in WT Th9 cells was selected for further analysis. Motif analysis of cell-specific peaks was done using HOMER. Other downstream analysis and heatmap generation were performed with R 3.0.1 and morpheus. For downstream analysis, regulatory elements were designated as promoters if they were located <2kb from the transcription start site (TSS) and as enhancers if located >2kb from the TSS.

Statistical Analysis of RNA-seq, qPCR, Flow Cytometry, and *In Vivo* Experiments

For 3C, ChIP-qPCR and luciferase assay, statistical significance was calculated by unpaired two-tailed Student's t-test with Graphpad Prism software. For T-cell intracellular cytokine production and dose-response curves, statistical significance was calculated using a paired two-tailed Student's t-test with Graphpad Prism software. For *in vivo* experiments, statistical significance was calculated using Mann-Whitney analysis with Graphpad Prism Software. For determination of differentially expressed genes from RNA-seq data, all statistical analysis was performed in Partek using Analysis of Variation (ANOVA), with multiple comparison adjustment to calculate false discovery rate (FDR). For ecdf plots, statistical analysis was done using Kolmogorov-smirnov testing in RStudio. For analysis of GSE73482, paired t-test was performed in Partek, with multiple comparison adjustment to calculate FDR.

Scoring: Papain- and Ova-Induced Asthma

Lung histology was scored on H&E and Periodic Acid Schiff (PAS) stained sections by a reader with experimental conditions masked, Perivascular and peri-bronchiolar cuffing (PVC and PBC) were each scored as follows: 0: No visible infiltrate. 1: Patchy infiltrate in <25% of bronchioles or vessels, 2: Patchy infiltrate in <50% of bronchioles or vessels, 3: Widespread infiltrate >50% of bronchioles or vessels with circumferential infiltrates in most bronchioles or vessels. 4. Criteria for score of 3 plus vascular obliteration (for PVC) or bronchiolar plugging (for PBC). Interstitial inflammation was graded from 0-3 depending on the extent of cellular infiltrate into alveoli. Goblet cell hyperplasia was scored for small airways as follows: 0: No visible hyperplasia or mucus production, 1: patchy hyperplasia and/or PAS staining in <25% of bronchioles or vessels, not circumferential, 2: patchy hyperplasia and/or PAS staining of <50% of bronchioles, 3: widespread hyperplasia and >50% PAS staining in most bronchioles, 4: criteria for 3 plus bronchiolar plugging or obliteration. Scores reported were the total score for each lung (0-15).

DATA AND SOFTWARE AVAILABILITY

The accession number for the data reported in this paper is GEO: GSE123501.